DYNAMIC ILLUMINATION SYSTEMS USING FREEFORM OPTICS

by

Shohreh Shadalou

A dissertation submitted to the faculty of
The University of North Carolina at Charlotte
in partial fulfillment of the requirements
for the degree of Doctor of Philosophy in
Optical Science and Engineering

Charlotte

2022

Approved by:

_____
Dr. Thomas Suleski

_____
Dr. Glenn Boreman

_____
Dr. Rosario Porras-Aguilar

_____
Dr. Matt Davies

ABSTRACT

SHOHREH SHADALOU. Dynamic Illumination Systems using Freeform Optics.
(Under the direction of DR. THOMAS J. SULESKI)

Illumination systems that can create light patterns of varying sizes or shapes with high efficiency and uniformity are advantageous for a range of applications, including lighting, augmented/virtual reality, laser-based manufacturing, medicine/dermatology, and lithography. Previous approaches for continuous variable illumination have utilized longitudinal movement of the source or other optical components along the optical axis, which increases both system size and light pattern non-uniformity. Liquid lenses with adjustable membranes have also been used for tunable illumination, but leakage and manufacturing complexity can be significant issues. Thus, new approaches that enable dynamically tunable illumination patterns in compact, robust packages are of interest.

Recent advances in design, production and metrology have enabled the use of freeform surfaces in a wide range of optical imaging applications. As one example, the Alvarez lens consists of a pair of cubic freeform surfaces that enable variable focal length with small lateral displacements between the two elements. Complex freeform surfaces are also regularly used in static illumination systems such as automotive headlights and luminaires.

The primary objectives of this dissertation are to explore and characterize dynamic freeform optical systems enabling continuously variable illumination. Results are addressed through three articles. The first article introduces the use of arrays of freeform Alvarez lenses with LED sources to enable tunable illumination. The second article builds from this work to present the design, manufacturing, and characterization of a compact tunable illumination system. The third article introduces a general design method using

freeform optics to enable variable optical illumination between two arbitrary boundary conditions. These three articles demonstrate the methods and utility of freeform optics for dynamic illumination systems.

ACKNOWLEDGEMENTS

I would like to express my gratitude to all the people who supported me and made my PhD journey enjoyable and memorable.

First and foremost, sincere gratitude to my adviser, Dr. Thomas Suleski, who brought my research to a higher level by his insightful guidance and profound knowledge. Without his continuous support, patience, and encouragement, I would not have been where I am now. I would also like to express my appreciation to my committee members, Dr. Glenn Boreman, Dr. Rosario Porras-Aguilar and Dr. Matthew Davies for their valuable feedback and advice.

I would like to appreciate Dr. Farahi who helped me have a better insight on how my mechanical engineering background can help me be prominent in the field of optical engineering. I am also grateful to Dr. Ronald Smelser, Dr. Harish Cherukuri, and Mrs. Tracy Beauregard in mechanical engineering department for their support to smooth my path towards the optical engineering program. My extended gratitude to Dr. Allen and Mr. Mark Clayton for helping me through my PhD application and welcoming me to the PhD program. I would also like to thank all my friends for making my PhD journey even more delightful, particularly Dr. Sara Moein, for our helpful conversation about dynamic freeforms in our teatime and having her company in different conferences.

Many thanks to Center for Freeform Optics (CeFO) and its members, both from academia and industry. CeFo provided me with funding for my research. Most importantly, its members provided deep constructive criticism which guided the project toward its perfection. I would also like to thank Dr. Casserly and Dr. Menke for mentoring the project within the CeFO. Their insights on the industry trends and professional software tools

helped me direct my research to better target our industrial community's state of the art needs. Additional thanks to Dr. Matt Davies and his former graduate student Dr. Dustin Gurganus for their collaboration on optomechanical design and fabrication of a demonstrator designed in this research.

My special appreciation goes to my family. My father, who is not in this world but lives in my heart; my mother, for having a deep belief in my potentials and raising me up to be who I am, with all hardship a single mom would have; my daughter Lenna for empowering me to study hard by her sweetest smiles and leaving sticker notes on my laptop saying "Love you mommy! You can do it!"; my son Liam who charged me with his lovely hugs and kisses; my beloved Masoud for being by my side in comfort and hardship and helping me grow towards the best of me: we migrated together, studied together, formed a lovely family together, and wish for making bright years ahead of us to achieve our dreams.

DEDICATION

To girls who never give up their dreams….

TABLE OF CONTENTS

LIST OF TABLES

LIST OF FIGURES

LIST OF ABBREVIATIONS

AD	Average Deviation
AR	Augmented Reality
CMOS	Complementary Metal Oxide Semiconductor
PMMA	Poly Methyl Methacrylate
PV	Peak to Valley
CNC	Computer Numerically Controlled
COTS	Commercial-Off-The-Shelf
FFD	Freeform Design
FWHM	Full Width at Half Maximum
LED	Light Emitting Diode
VR	Virtual Reality
ROC	Radius of Curvature
Sa	Surface Roughness
TIR	Total Internal Reflection

CHAPTER 1: INTRODUCTION

1.1 Background and motivation: Tunable illumination

Increased usage of engineered light distributions in recent years for multiple applications has resulted in substantial advancements in 'non-imaging' optical systems [1-4]. The engineering process of transporting light from a source(s) to the desired target is known as *illumination design* [2]. Illumination systems capable of providing spatial light distribution with continuously variable sizes or shapes can be beneficial for many applications, including advanced lighting, automotive, microscopy, AR/VR, medicine/dermatology, beam shaping, and lithography. Light distributions with high uniformity are also desired to avoid illumination defects impacting system performance or visual perception [5].

Variable illumination has been previously achieved by simply moving the source(s) or other optical components longitudinally along the optical axis. However, this approach typically increases non-uniformity or other undesired defects in the illumination pattern [6, 7]. Zoom lens systems involving multiple optics may be used in illumination systems to provide better control on the light distribution but can require bulky structures which limits the implementation in modern compact optical systems [8].

Another method to add variable functionality to illumination systems utilizes liquid lenses, which adjust optical power and consequently illumination size by modulating lens curvature or refractive index. Lens curvature can be tuned through different approaches including membrane deformation and the electrowetting effect [9-13]. The refractive index can be adjusted in liquid crystal lenses by varying the orientations of the liquid crystal directors using an inhomogeneous electric field [14-18]. While the use of liquid lenses

generally provides a high tuning range of optical power, it also introduces potential disadvantages such as leakage, evaporation, manufacturing complexity, temperature, gravity sensitivities, and performance instabilities [19]. In recent years, novel forms of deformable elastomeric lenses have received great interest, with clear benefits over liquid tunable lenses including higher mechanical and thermal stability. However, high material stiffness limits their tuning range [20-22].

In general, direct use of tunable optical power in conjunction with non-uniform optical sources in illumination systems results in non-uniform output patterns, especially when a large tuning range is required. Use of a plurality of sources [23-26] or integrated lens arrays [27-31] can enhance the uniformity and provide more homogenized outputs. Array arrangements can also be used to engineer the shapes of light distributions using edge ray theory and convolution principles [32, 33].

1.2 Background and motivation: Freeform optics for tunable illumination

Advances in design, high-precision manufacturing, and metrology techniques have facilitated the implementation of freeform surfaces in optical systems [34-38]. Freeform optical surfaces reduce limits imposed by rotationally symmetric optics and provide extra degrees of freedom to optical designers. Among many, many other applications, the extra design freedoms enabled by freeform optics can provide potential benefits for managing the tunability, uniformity, and shape of illumination patterns.

One type of lens system employs refractive pairs capable of generating constantly varying optical power through lateral shifts between the elements in a transverse plane relative to the optical axis. Early approaches relied on a direct superposition concept, in

which the output wavefront could be considered as a superposition of the individual wavefront deformations from passing through each individual refractive plate [39-41]. The first documented design is attributed to Kitajima for an adjustable optical power system using two orthogonally-shifted cylinder lenses with varying radii of curvature [39]. The composite wavefront varies as lateral shifts are applied to the optical components. Although this approach has been reported to provide dynamic illumination, distortion defects caused by non-uniform optical power across the aperture and the need for relatively large lateral shifts are not conducive for practical implementation [42].

The next generation of dynamic optics was enabled using an integral method with pairs of plano-freeform refractive elements. By applying lateral relative shifts in opposite directions to freeform pairs with matching surfaces, the output wavefront deformation can be related to the derivative of the individual freeform surfaces and the amount of applied shift [43-49]; the matching freeform surfaces in these systems are related to the integral of the of desired wavefront. This approach was initially presented by Alvarez and Lohman independently in 1970 [43, 44]. The so-called 'Alvarez lens' consists of two freeform elements with matching cubic surfaces that generate variable spherical power as opposite lateral shifts are applied to the components. This concept was further generalized by Palusinski *et al* in 1999 and employed to design variable aberration generators [50]. Although this design approach results in no optical power at zero shift, several works have reported on adjusting the working range [51-56].

In comparison to the direct superposition method discussed previously, the integration approach requires significantly smaller lateral shifts while causing considerably less distortion. In general, Alvarez lenses can enable more compact and tunable optical systems

than zoom lenses and provide wider tuning ranges than adaptive elastomer lenses. Tunable systems based on Alvarez lenses are also more stable than systems using liquid lenses since issues with sealing, evaporation and related challenges are removed.

As with other optical systems that may be used to enable dynamic illumination, direct use of Alvarez lenses can result in undesirable non-uniformity. As discussed previously, array configurations have been used to enhance illumination uniformity. However, while the use of array configurations has also been extended to freeform optics [55-57]; However, use of Alvarez arrays in dynamic illumination system providing high uniformity has not been previously reported in the literature.

The use of freeform optics coupled with LED and laser beam sources to improve the uniformity or obtain prescribed target patterns has attracted significant interest among illumination designers in recent years [58-60]. Wu *et al* in [58] reviewed freeform design methods to enable prescribed illumination including ray mapping [61-63], Monge-Ampère [64-66], supporting quadric [67, 68], optimization [4, 69, 70], feedback design [71], and Simultaneous Multiple Surfaces (SMS) approaches [72, 73]. Variable illumination modes have been previously enabled by switching optical components [74-76]. However, the design of dynamic freeform illumination systems to enable continuously variable optical performance is challenging and has received limited attention to date.

Researchers recently reported dynamic beam shaping elements based on the Alvarez concept to transform a radially symmetric Gaussian input beam into uniform irradiance outputs of different shapes and sizes [77-80]. Although the reported results are very promising, the method requires multiple intermediate static designs and curve fits that can be time-consuming and assumes similar optical functionality across the variable range.

Defining multiple target patterns in advance is also challenging for cases having non-linear relations between shift and target size. A freeform design method capable of varying optical performance between two arbitrary boundary conditions without the need for intermediate static designs could be an ideal solution for illumination designers working on advanced applications but has not been previously reported.

1.3 Dissertation outline

Chapter 2 introduces and explores the use of varifocal transmissive freeform Alvarez lens arrays for a tunable LED-based lighting system. The design is initiated using paraxial geometrical optics concepts and then enhanced using a white LED model in a multi-step optimization process. Design processes and simulation results for a lighting system with outputs varying from a small circular spot mode to a large square uniform flood mode through millimeter-scale lateral translation between the Alvarez lens arrays are presented.

Chapter 3 builds from the work from Chapter 2 to report on the fabrication and experimental characterization of a variable freeform illumination system. Commercially available components are used in conjunction with custom freeform Alvarez arrays to shorten the building process for the demonstrator. Design and manufacturing processes are presented for the custom Alvarez arrays and optomechanical fixtures for the demonstrator. A custom camera-based test station and analysis software are developed and implemented to characterize the optical performance of the illumination system.

Chapter 4 introduces a general design method for refractive two-element systems to enable variable optical performance between two specified boundary conditions. As with the Alvarez lens, the pair of plano-freeform elements is subjected to small, relative lateral shifts in opposing directions. In contrast to prior techniques, this method is not confined to

boundaries with similar optical functions and can enable a broad variety of difficult, dynamic functions for both imaging and non-imaging applications. Theoretical foundations and design processes are discussed for both analytical and numerical implementations. Numerous examples are provided to illustrate the versatility of the new method.

CHAPTER 2: TUNABLE ILLUMINATION FOR LED-BASED SYSTEMS USING REFRACTIVE FREEFORM ARRAYS [81]

2.1 Abstract

Tunable illumination with high uniformity can improve functionality for multiple application areas. In lighting applications, dynamic illumination has been achieved by applying axial movement to the source(s) or other optical elements, resulting in poor uniformity, or using a liquid lens that adds design complexity. Advances in high-precision manufacturing methods have facilitated the practical implementation of freeform optical components, enabling new design approaches for illumination systems. This paper explores the use of arrays of varifocal transmissive freeform Alvarez lenses for an LED-based illumination system. The design is initialized using paraxial geometrical optics concepts and then refined for a 1mm-by-1 mm white LED source through a multi-step optimization. Design procedures are discussed, and simulation results are presented for an example illumination system that varies from a small circular spot mode to a large square uniform flood mode through millimeter-scale lateral translation between the Alvarez lens arrays.

2.2 Introduction

Illumination systems with the ability to provide spatial light distribution with continuously variable size can be beneficial for multiple applications such as advanced lighting, entertainment, medicine, automotive, and security. High uniformity is desirable to avoid illumination defects that can impact system performance or visual perception [1]. Design of illumination systems with high efficiency is also desirable for energy

conservation. Modern illumination systems commonly use light-emitting diode (LED) sources, which significantly enhance lighting efficiency. In addition to low power consumption, LED sources offer high reliability, controllability, and long lifetimes [2].

Variably sized illumination patterns have been previously achieved, for example, by applying longitudinal movements along the optical axis of the system to the source(s) or other optical elements [3-6]. However, the chance of experiencing non-uniformity in the illuminance pattern is high. Uniformity in illumination systems can be improved, for example by using a plurality of sources [7-10] or by using integrating lens arrays [11-13]. The arrangement of lenses or source arrays is an important factor in the design of such systems that impacts the shape of output illuminance patterns [14] as well as system size. Utilizing multiple LEDs or using lens arrays in a zoom arrangement enhances uniformity but may not result in sufficiently compact systems for some applications.

Improvements in high-precision manufacturing techniques such as diamond machining have facilitated the implementation of freeform optics in optical systems. Freeform optics offer additional design freedoms in the absence of constraints imposed by rotationally symmetric optics [15]. The use of freeform optics in illumination systems to provide prescribed illuminance patterns has also gained significant interest among designers [16]. Freeform design has also enabled highly uniform illuminance patterns from LED sources with non-uniform Lambertian distribution [17-20]. To improve the functionality in illumination systems, researchers have proposed LED-based illumination systems with multiple operating modes using freeform optics [21, 22]. However, these approaches cannot provide continuously tunable illumination. Researchers have previously reported refractive two-element systems based on freeform optics converting Gaussian laser

distribution to flat-top outputs with adjustable diameter [23, 24]. However, this approach is based on monochromatic, collimated, Gaussian beams, but LEDs have non-collimated Lambertian light distributions. Reviewing the literature shows that continuously variable illumination in LED-based systems using freeform optics has not received sufficient attention.

We previously reported a dynamic illuminator based on a parabolic reflector, a pair of fixed confocal lens arrays, and an array of freeform Alvarez lenses, as can be seen in Fig. 1(a) [25]. In that system, the light incident on the Alvarez lenses is collimated and the Alvarez lenses provide variable spherical power through lateral relative translation between pairs of plano-freeform elements [26]. The use of arrays in the design enhances uniformity while also reducing the maximum lateral shift needed between the freeform elements. This system demonstrates dynamic illumination from spot mode to a homogenized flood mode, but the system assumes a point source and uses a limited scanning range of the Alvarez arrays.

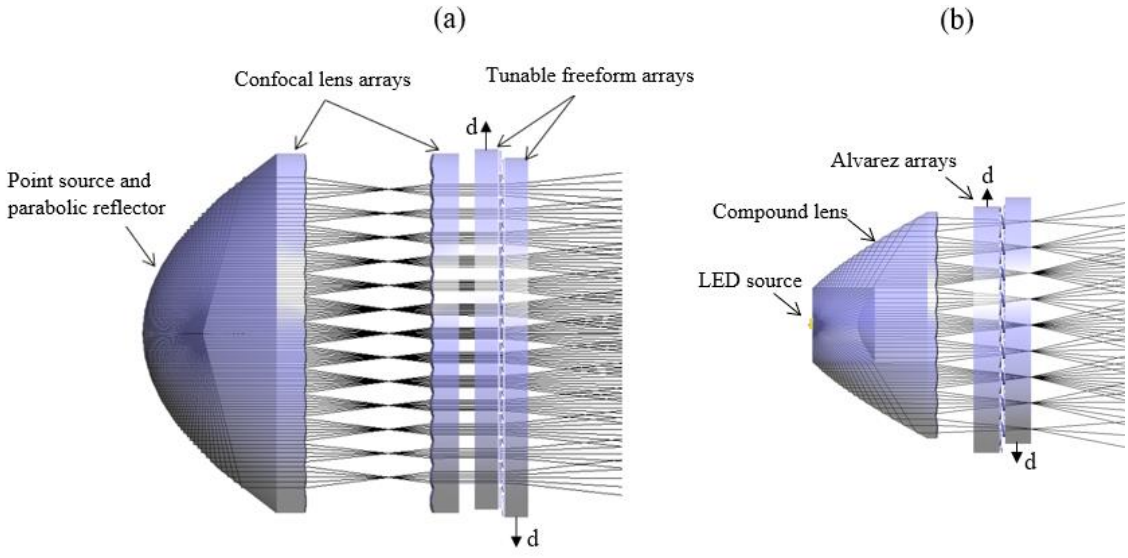

Fig. 2.1. (a) Schematic of dynamic illumination design from [25]; (b) Tunable LED-based illumination system based on convergent ray bundles.

In this paper, we present a compact tunable illuminator shown in Fig. 2.1(b) using a real LED source, a compound optic consisting of a total internal reflection (TIR) lens with an integrated lens array, and arrays of Alvarez lenses. The use of the compound optic reduces the number of components and creates convergent ray bundles that extend the practical working range of the Alvarez arrays and results in a more compact system. The initial design is constructed by assuming a point source and applying paraxial geometrical optics concepts. A simultaneous optimization approach is then demonstrated to expand and enhance the performance of the design based on a real LED [27].

Section 2.3 presents the general design approach and background information. This approach is demonstrated in detail through a design example in Section 2.4. Simulation results are discussed in Section 2.5, followed by conclusions in Section 2.6.

2.3. General design approach

This work combines two main concepts: (1) homogenizing the illuminance pattern using an integrated lens array, and (2) generating variable divergence illumination utilizing arrays of freeform Alvarez lenses.

A lens array can be combined with a collimator to generate a homogenized illuminance pattern from a non-collimated source. Using a TIR lens is a common approach to collimate a LED light distribution. Besides uniformity, different arrangements of lenses in the array (e.g., rectangular, hexagonal, and so on) enable generation of various shapes of illuminance patterns. This behavior can be explained by considering the target pattern as a convolution of the source intensity and lenslet response. The lenslet response depends on the aperture shape and curvature of each lenslet [14].

Alvarez lens arrays [e.g., 28, 29] can be used in an illumination system to enable tunability while also reducing the system size compared to a single pair of Alvarez lenses. The general form of the Alvarez lens pairs consists of two plano-freeform elements with matching cubic surfaces resulting in a continuously variable spherical power as opposite lateral shifts are applied. The freeform surface equation following a first-order analytical approach is given by:

$$z(x, y) = A(\frac{x^3}{3} + xy^2) + Cx, \quad (2.1)$$

where z corresponds to the surface thickness, coefficient A controls the depth modulation of the surface, and coefficient C is a prism term impacting the element's thickness. The equivalent optical power P for the composite surface is then:

$$P = -4Ad(n_m - n_s), \quad (2.2)$$

where d is the lateral shift of each freeform element along the x direction and nm and ns are the refractive indices of the optical material and surrounding medium. This general form generates positive, negative, or zero optical power at negative, positive, and zero lateral shifts of the elements, respectively [26].

The use of Alvarez lens pairs with collimated light results in the minimum divergence angle (spot mode) to occur with no shift between the Alvarez lenslets (Fig. 2.2(a)). A similar spread (flood mode) is achieved with both positive and negative lens shifts. To ensure that only the overlap area of the Alvarez lenses is illuminated, additional array optics are used. This was done using two lens surfaces in the previous system [25]. An alternative approach is to use a converging beam to illuminate the Alvarez lenses so that the collimated beam (spot mode) occurs with the lenses shifted in the positive direction (Fig. 2.2(b)). This

means the negative shift can produce an even wider beam spread (flood mode) compared to the conventional layout.

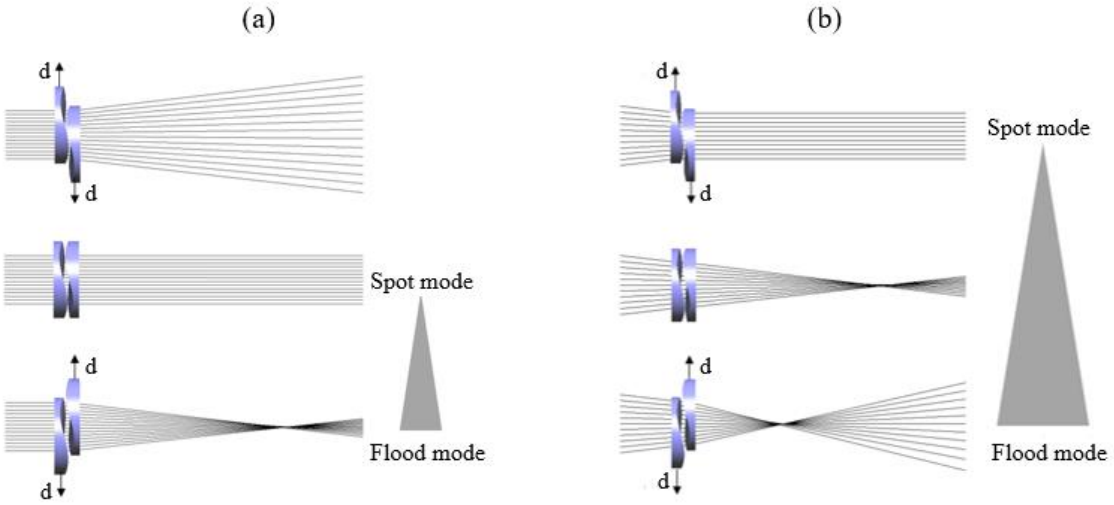

Fig. 2. 2. Alvarez lens pair with (a) parallel incident ray bundle and (b) convergent ray bundle.

Based on the presented design ideas, light emitted from a Lambertian LED is considered to pass through a collimator and be redistributed into convergent ray bundles by an integrated lens array. Each of these convergent channels then enters a unit cell in the Alvarez arrays, and their angular path is adjusted by applying lateral relative shifts to the Alvarez freeform lenses.

A model of the illuminator including the source, collimator, and Alvarez arrays can be constructed in optical software. The initial design parameters can be calculated by applying paraxial geometrical optics concepts to edge rays passing through a single unit at the boundary conditions. Fig. 2.3 shows a single converging ray bundle from a lenslet of power P1 that is adjusted to the final viewing angle by passing through the shifted Alvarez lens pair with power $-P_2$ for spot mode and power P_2 for flood mode. The incident angle of the

edge ray for the collimated ray bundle (u_1) is zero and the refracted angles for the spot and flood modes can be calculated based on the target geometry.

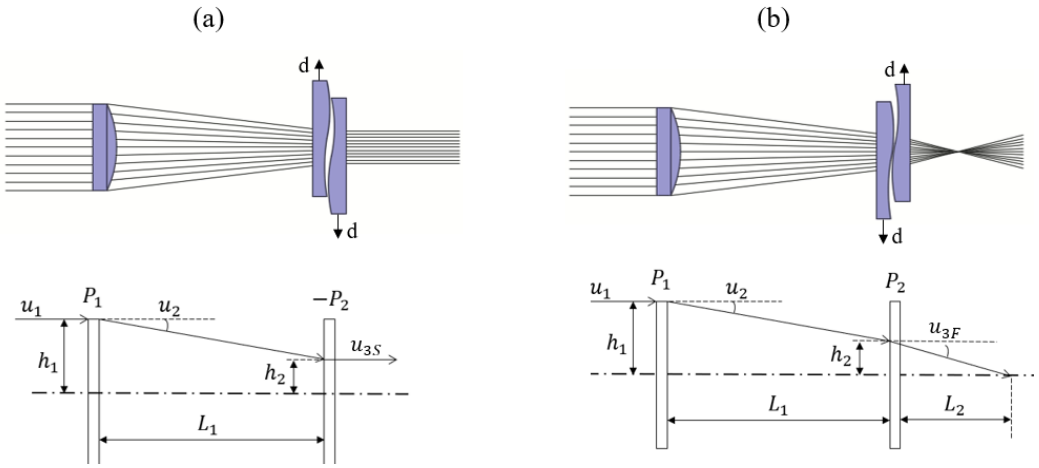

Fig. 2.3. Edge ray trace at boundary conditions: (a) spot mode, and (b) flood mode.

The edge ray geometries are the same in both spot and flood modes before entering the Alvarez lens. The refracted angle of the edge ray u_2 from the plano-convex lenslet and its height (h_2) before entering the Alvarez lens are given respectively from the transfer function as:

$$u_2 = u_1 - P_1 h_1, \tag{2.3}$$

$$h_2 = h_1 - u_2 L_1, \tag{2.4}$$

where P_1 is the optical power of the lenslet and L_1 is the distance between the lenslet and the Alvarez lens. After passing the Alvarez lens pair, the refracted angles of the edge rays for spot mode (u_{3S}) and flood mode (u_{3F}) are respectively:

$$u_{3S} = -u_2 + P_2 h_2, \tag{2.5}$$

$$u_{3F} = -u_2 - P_2 h_2. \tag{2.6}$$

Using Eqs. (2.3) to (2.6), we calculate the optical power of the lenslet (P_1), the maximum optical power of the Alvarez lens pairs (P_2), and the distance between them (L_1), respectively as:

$$P_1 = \frac{(2u_2 + u_{3S} + u_{3F})}{2h_1}, \tag{2.7}$$

$$P_2 = \frac{u_{3F} - u_{3S}}{2h_2}, \tag{2.8}$$

$$L_1 = \frac{2(h_1 - h_2)}{u_{3S} + u_{3F}}. \tag{2.9}$$

The radius of curvature (R) of the lenslets can be found by applying the lens-maker's equation to Eq. (2.7):

$$R = \frac{2h_1(n_m - n_s)}{2u_1 + u_{3S} + u_{3F}}. \tag{2.10}$$

The A coefficient of the Alvarez surface can then be obtained using Eq. (2.2) and (2.8):

$$A = \frac{u_{3F} - u_{3S}}{8h_2 d_{\max}(n_m - n_s)}. \tag{2.11}$$

The required values u_{3S}, u_{3F}, h_1, and h_2 needed to calculate the main design parameters are set by the requirement of the illumination system. The main design parameters obtained from the above paraxial calculations provide a starting design for the optical system. The design process can be accelerated by using multi-step optimizations beginning with an infinitesimal monochromatic Lambertian source and a small number of rays continuing with gradually increasing the number of beams and replacing the point source with a real

LED model [27]. The full design process is illustrated in more detail through an example in the next section.

2. 4 Design example

We next apply the approach presented in Section 2.3 to the conceptual design of a desk lamp. the goal of this design is to generate continuous variable illumination from spot mode to uniform square shape (w = 1000mm) flood mode over a desk at a fixed distance of h = 2000 mm from the LED source, as illustrated in Fig. 2.4.

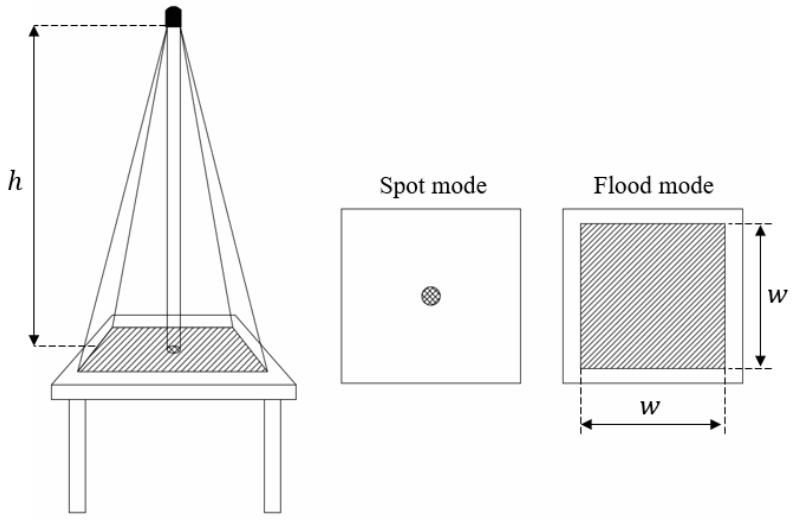

Fig. 2.4. Schematic of a variable illumination desk lamp used as a design example.

As discussed in Section 2.3, the dynamic illumination system includes a Lambertian LED source, a TIR lens to collimate the light, a lens array to distribute the light into the convergent ray bundles, and Alvarez arrays to dynamically control the size of the illumination pattern.

The first step in the design is initializing the main design parameters. For the current design, the size of each unit is 4 mm-by-4 mm, and the Alvarez lens clear aperture is 1.5mm-by-1.5mm. Therefore, h1 and h2 are 2mm and 0.75mm, respectively. The

maximum shift d of the Alvarez arrays is set as ±0.7mm. The design material is polycarbonate, and the space material is air (refractive indices of 1.5968 and 1, respectively). Based on the target geometry, the desired half-viewing angle from the illuminator at flood mode (u_{3F}) is equal to w/2h and for the spot mode $u_{3S} = 0$. Considering these assumptions and using Eqs. (2.9) to (2.11), for the lenslets R = 9.44 mm, the optical distance between the lenslet array and Alvarez arrays (L_1) is 10mm, and the A coefficient for the Alvarez surface is 0.1 mm^{-2}. These values are used as initial parameters for the design.

For the source, we selected a Lambertian white light LED from the default library of LightTools® with the following specifications: flux = 148 Lumens, viewing angle = 120°, chip LED size 1mm-by-1mm. We then designed a compound lens, including the TIR lens and lens array. The "LED lens design" feature in LightTools™ was used to develop the TIR lens. The lens array was modeled by creating a cylindrical base and adding a spherical bump 3D texture with unit size of 4mm-by-4mm. This lens array was immersed in the TIR lens to serve as one compound element, as illustrated in Fig. 2.5.

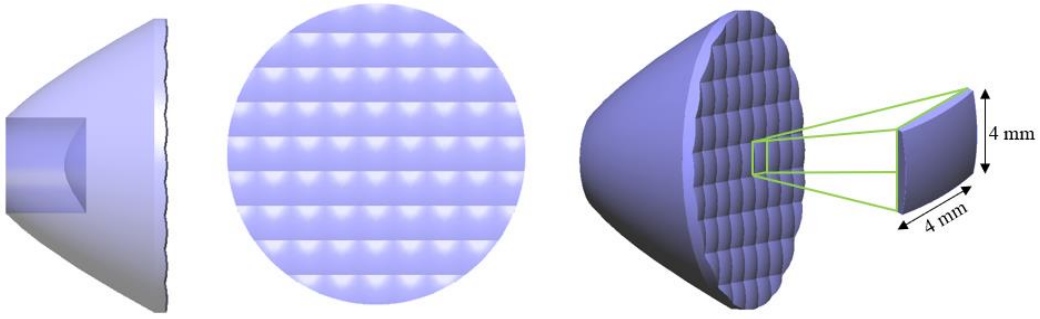

Fig. 2.5. 3D model of TIR lens with an integrated lens array in LightTools™.

The Alvarez arrays were realized in LightTools™ by first creating a unit cell consisting of a single Alvarez lens. The freeform surface is specified by a polynomial equation, as discussed in Section 2.3. The circular Alvarez lens was intersected by a mechanical element with the desired geometry to construct an oval-shaped Alvarez lens with major axis of 3.8 mm and minor axis of 2.5 mm which takes the 1D lateral shift into consideration. The oval shape of the Alvarez lens minimizes the overall depth modulation and limits the precise manufacturing area to the required clear aperture. The Alvarez arrays were constructed in LightTools™ by adding a 3D texture of a single Alvarez lens as a library element to a cylindrical flat base, as shown in Fig. 2.6.

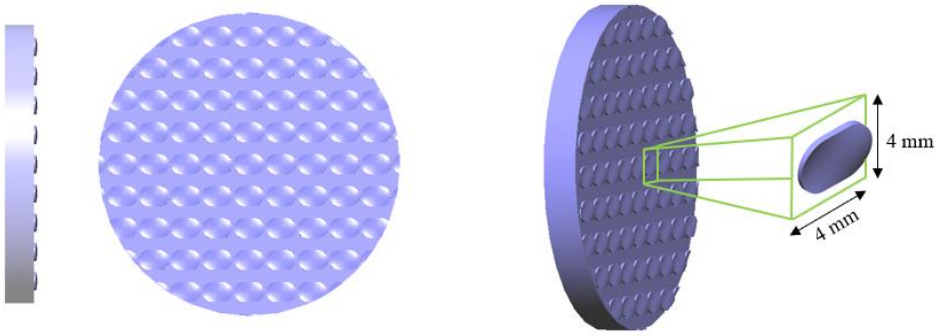

Fig. 2.6. 3D model of first Alvarez array in LightTools®.

We next created two parallel configurations associated with the spot and flood modes using the initial calculated design parameters and corresponding to the maximum lateral shifts of the Alvarez arrays (+0.7 mm for the spot mode and -0.7 mm for the flood mode, respectively) for simulation in LightTools™. We added filters to the plane receivers and pickups to the optimization variables to connect these configurations. The collimated merit function was set for the spot mode configuration, and a uniform square-shaped mesh merit function was set for the flood mode configuration to perform the simultaneous Monte Carlo optimization. The first optimization step was based on an ideal monochromatic (550nm)

infinitesimal Lambertian source. Further optimizations were performed while gradually increasing the number of rays and replacing the source with a real LED. The resulting final geometry is shown in Fig. 2.7.

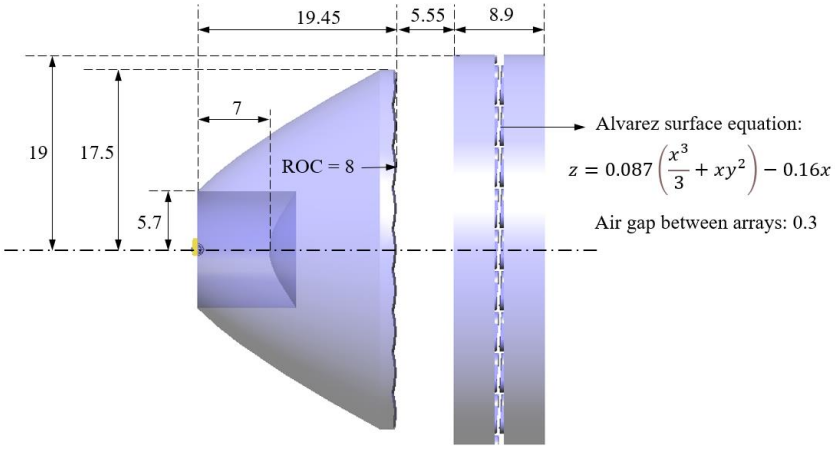

Fig. 2.7. The final geometry of the tunable illumination system after optimization (all units in mm).

2. 5 Simulation results

Simulation results for a design example show a continuously variable illuminance pattern from a circular spot mode to a homogenized square flood mode from a 1mm-by-1mm white LED source. The full width at half maximum (FWHM) in the x-direction throughout the entire shift range of the Alvarez arrays is shown in Fig. 2.8.

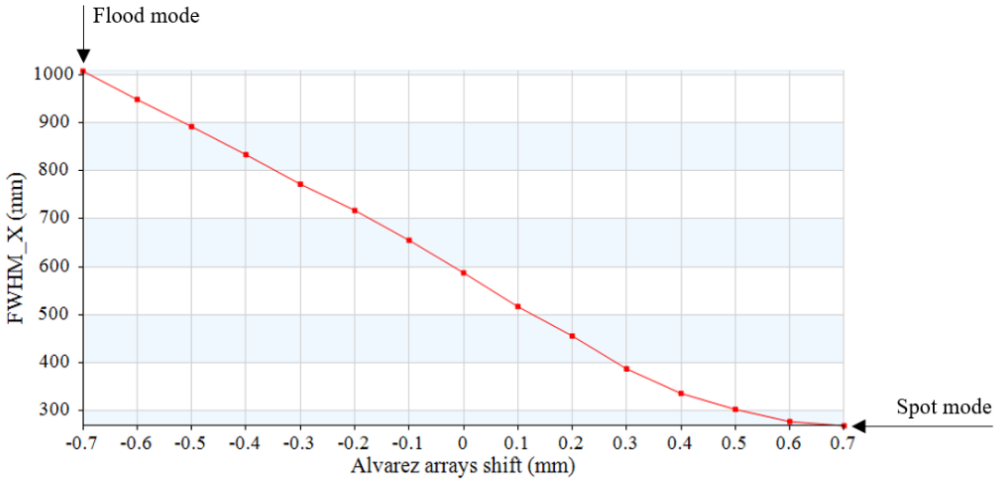

Fig. 2.8. FWHM(x) as a function of Alvarez shift (*d*).

Simulated true color and illuminance patterns for three selected modes within the continuous variable illumination range after tracing 1,000,000 rays through the system are shown in Fig. 2.9. The true color image shows good color homogeneity from the white LED source. The sizes of the illuminance patterns for these three modes are listed in Table 2. 1.

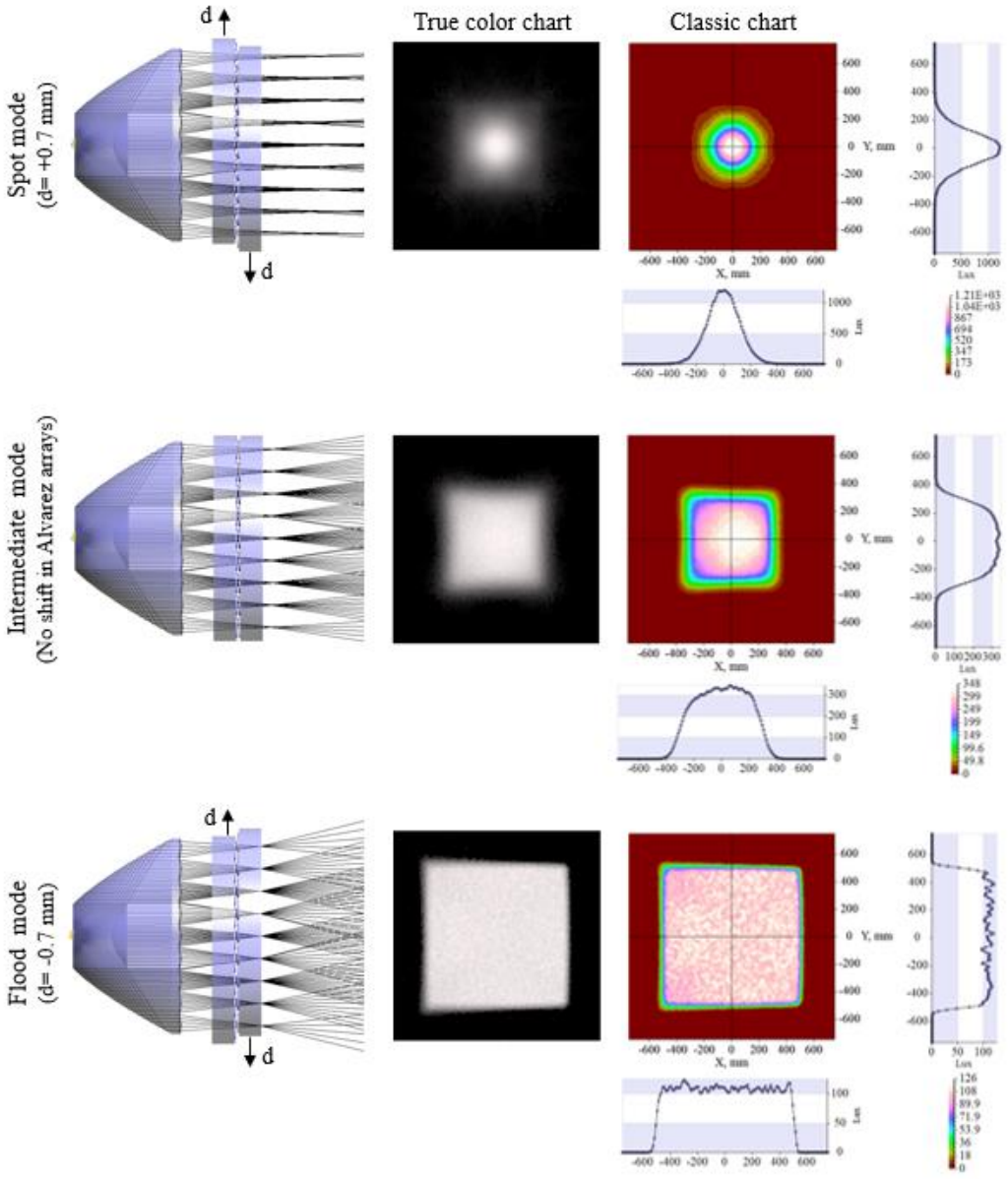

Fig. 2.9. True color and illuminance patterns of spot, intermediate, and flood modes at 2000 mm from the source.

Table 2. 1. Width at 50% of the center value (FWHM).

Mode name	Alvarez array shift (dx)	FWHM along x	FWHM along y	Average FWHM
Spot	+0.7 mm	---	---	270 mm
Intermediate	0	587mm	580 mm	---
Flood	-0.7 mm	1007 mm	1007 mm	---

The simulation results show the expected square distribution shape in flood mode because the lenslets are imaged onto the target and the source size only has a small effect. Other flood distribution shapes could be achieved by changing the shape of the lenslets in the lens array (e.g., hexagonal, or rectangular).

When moving from flood mode towards spot mode, the size of the extended source becomes increasingly important since the TIR collimator must conserve etendue [30] and does not provide perfect collimation. Notice that the edges of the square pattern in intermediate mode are smeared more than in flood mode. In spot mode, there is additional smearing due to the extended source, with the result of a somewhat rotationally symmetric Gaussian distribution.

The Average Deviation (AD), defined as (standard deviation/average illuminance), was used to provide a quantitative evaluation of the uniformity of the illuminance patterns. Zero AD corresponds to a perfectly uniform pattern. A circular aperture was used for the spot mode and a square aperture for the flood mode for the uniformity calculations. The values of AD over the apertures with the target patterns' exact size are listed in Table 2. **2**. The significant value of AD for the flood mode is due primarily to the edge of the pattern.

Table 2. 2. Mesh data of illuminance patterns over the target areas.

Illumination mode	Aperture geometry	Average illuminance	Average deviation
Spot mode	Circle with a diameter of 270 mm	838 Lux	28%
Flood mode	Square with a side of 1000 mm	104 Lux	12%

2.6 Conclusion

A general design approach has been presented that enables dynamic variation of illumination patterns with high uniformity in an LED-based system using arrays of freeform Alvarez lenses. Convergent light channels from an LED source were created using a TIR lens combined with a lens array to utilize the entire working range of the Alvarez arrays in varying from spot mode to flood mode in the example illumination system. The change in beam width between spot and flood mode is maximized by illuminating the Alvarez array with converging wave fronts. This system enables dynamic illumination with high uniformity along the working range through millimeter-scale lateral shifts to the Alvarez arrays, which is beneficial for applications where the system size and dynamic range of physical movement are limited. The exit surface for this system is also planar and easy to clean.

The starting point for the design was defined by applying paraxial geometrical optics concepts to the system's boundary conditions based on the design application, followed by a simultaneous Monte Carlo optimization over the spot and flood mode to achieve the desired targets. The optimization process begins with an infinitesimal monochromatic Lambertian source and a small number of rays, followed with gradually increasing the number of rays and replacing the source with a real LED model. Simulation results show that the system meets the desired design goals with good uniformity. Additional work to fabricate and experimentally characterize the performance of the system is underway.

2. 7 References

1. J. Whang, S. M. Chao, C. N. Chen, Y. Y. Chen, H. C. Hsiao, and X. D. Hu, "High uniform illumination of light-emitting diodes lighting with applying the multiple-curvature lens," Opt. Rev. 18, 218-223 (2011).
2. J. M. Gee, J. Y. Tsao, and J. A. Simmons, "Prospects for LED lighting," Proc. SPIE 5187, 227-233 (2004).
3. R. D. White and D. P. Weiss, "Lighting device with dynamic bulb position," U.S. patent 4,339,788 (3 July 1982).
4. S. S. Shiau, "Variable focusing flashlight," U.S. patent 5,213,408 A (25 May 1993).
5. Nemeyer, "Adjustable beam illuminator," U.S. patent 9,395,066 B2 (19 July 2016).
6. R. Opolka and A. Timinger, “LED illumination module,” U.S. patent 7,461,960 B2 (9 Dec 2008).
7. Moreno and R. I. Tzonchev, "Effects on illumination uniformity due to dilution on arrays of LEDs," Proc. SPIE 5529, 268-275 (2004).
8. J. Whang, Y. Y. Chen, and Y. T. Teng, "Designing uniform illumination systems by surface-tailored lens and configurations of LED arrays," J. Disp. Technol. 5, 94-103 (2009).
9. J. B. Lee, I. Brian, Y. Chiang, and H. K. Ho, "Zoom spotlight using LED array," U.S. patent 8,979,316 B2 (17 March 2015).
10. D. J. Stavely, "Variable focus illuminator," U.S. patent App. 2012/0121244 A1 (17 May 2012).
11. Harder, M. Lano, N. Lindlein, and J. Schwider, “Homogenization and beam shaping with microlens arrays,” Proc. SPIE 5456, 99-107 (2004).

12. T. R. Sales, "Random microlens array for optical beam shaping and homogenization," U.S. patent 6,859,326 (2 February 2005).
13. P. Schreiber, S. Kudaev, P. Dannberg, and U. D. Zeitner, "Homogeneous LED-illumination using microlens arrays," Proc. SPIE 5924, 59420K (2005).
14. P. Riser and W. J. Cassarly, "Analysis of single lens arrays using convolution," Opt. Eng. 40, 805-813 (2001).
15. J. P. Rolland, M. A. Davies, T. J. Suleski, C. Evans, A. Bauer, J. C. Lambropoulos, and K. Falaggis, "Freeform optics for imaging," Optica 8, 161-176 (2021).
16. R. Wu, Z. Feng, Z. Zheng, R. Liang, P. Benítez, J. C. Miñano, and F. Duerr, "Design of Freeform illumination optics," Laser Photonics Rev. 12, 1700310 (2018).
17. W. Tai, and R. Schwarte. "Design of an aspherical lens to generate a homogenous irradiance for three-dimensional sensors with a light-emitting-diode source." Appl. Opt. 39, 5801-5805 (2000).
18. F. Chen, S. Liu, K. Wang, Z. Liu, and X. Luo, "Free-form lenses for high illumination quality light-emitting diode MR16 lamps," Opt. Eng. 48, 123002 (2009).
19. H. Wu, X. Zhang, and P. Ge, "Double freeform surfaces lens design for LED uniform illumination with high distance–height ratio," Opt. Laser Technol. 73, 166-172 (2015).
20. J. Zeng, X. Li, and P. Ge, "Design of LED collimator for uniform illumination using two freeform lenses," Opt. Appl. 48, 413-420 (2018).

21. E. Juntunen, P. Myöhänen, E. Tetri, O. Tapaninen, J. Ojalehto, and V. Heikkinen, "Rapid prototyping of freeform optics for an LED downlighter with a dynamically adjustable beam," Light. Res. Technol. 48, 885-897 (2016).
22. D. Xin, H. Liu, L. Jing, Y. Wang, W. Xu, and Z. Lu, "Design of secondary optics for IRED in active night vision systems," Opt. Express 21, 1113-1120 (2013).
23. T. J. Suleski, P. J. Smilie, and J. A. Shultz, "Dynamic laser beam shaping methods and systems," U.S. patent 9,238,577 (19 January 2016).
24. P. J. Smilie, and T. J. Suleski. "Variable-diameter refractive beam shaping with freeform optical surfaces." Opt. Lett. 36, 4170-4172 (2011).
25. S. Shadalou and T. J. Suleski, "Freeform optics for dynamic illumination," Proc. SPIE 11495, 114950B (2020).
26. L. W. Alvarez and W. E. Humphrey, "Variable-power lens and system," U.S. Patent 3,507,565A (1970).
27. T. L. R. Davenport, T. A. Hough, and W. J. Cassarly, "Optimization for illumination systems: the next level of design," Proc. SPIE 5456, 81-90 (2004).
28. E. Acosta and J. Sasian, "Micro-Alvarez lenses for a tunable-dynamic-range Shack–Hartmann wavefront sensor," Jpn. J. Appl. Phys. 53, 08MG04 (2014).
29. Huang, L. Li, and A. Yi, "Design and fabrication of a micro Alvarez lens array with a variable focal length," Microsys. Techno. 15(4), 559-563 (2009).
30. R. J. Koshel, Illumination Engineering: Design with Nonimaging Optics (John Wiley and Sons: IEEE Press, 2013), Chap. 2.

CHAPTER 3: DESIGN, FABRICATION, AND CHARACTERIZATION OF TUNABLE LED-BASED ILLUMINATOR USING REFRACTIVE FREEFORM ARRAYS

3.1 Abstract

Dynamic illumination Dynamic illumination using tunable freeform arrays can enable spatial light distributions of variable size of with high uniformity from non-uniform sources through relatively small opposing lateral shifts applied to the freeform components. We present the design, manufacturing, and characterization of a tunable LED-based illuminator using custom freeform Alvarez arrays with commercially available optics to shorten the manufacturing cycle. The optomechanical design and manufacturing of Alvarez lens arrays and mounting parts are presented in detail. The optical performance of the system is evaluated and compared with simulation results using a developed camera-based test station and a test platform. Experimental results demonstrate and confirm the dynamic illumination concept with good uniformity.

3.2 Introduction

Most illumination systems assume static relationships between the input source and the output illuminance pattern. Continuously variable illumination patterns can be advantageous in a range of applications including, for example modern lighting, automotive, medicine, dermatology, and lithography. Output patterns with good uniformity are preferable to eliminate lighting faults that degrade system performance or visual perception [1]. Energy savings is also an important factor in the design of illumination systems, with light-emitting diode (LED) sources used to improve efficiency. In addition

to low power consumption, LEDs are more reliable, controllable, with longer life compared with traditional lighting sources [2].

Dynamic spatial light distribution for lighting application have been previously achieved by changing spacing between elements along the optical axis, which can result in undesirable pattern non-uniformity [3, 4]. Lens arrays may be used to help enhance homogeneity of the system, but the longitudinal shift may still be undesirable in some compact systems [5, 6]. Liquid lenses can also provide adjustable optical power with high tuning range [7-9]. However, such elements can results in disadvantages such as temperature and gravity sensitivities, sealing, and evaporation challenges [10]. Soft solid elastomer lenses can also provide tunable optical power but with a very limited tuning range due to high material stiffness [11, 12].

Advances in design, manufacturing, and precision metrology have enabled use of freeform optics in advanced system designs [13, 14]. As one example, freeform elements can enable tunability through the use of Alvarez lenses, which generate variable spherical power by relative lateral translation between a pair of plano-cubic elements in opposing directions [15]. However, coupling a single Alvarez lens to the non-uniform LED source does not improve uniformity. We previously reported the use of arrays of Alvarez lenses to address this issue for a tunable illumination system that enables continuous variable illumination from spot mode to uniform flood mode, as shown in Fig.1 [16]. The use of arrays enhances the uniformity of the target illuminance pattern, while the lateral (rather than longitudinal) shifts between components reduce the system package size. This approach enables the desired performance, but requires multiple custom components, which makes fabrication more difficult and time-consuming.

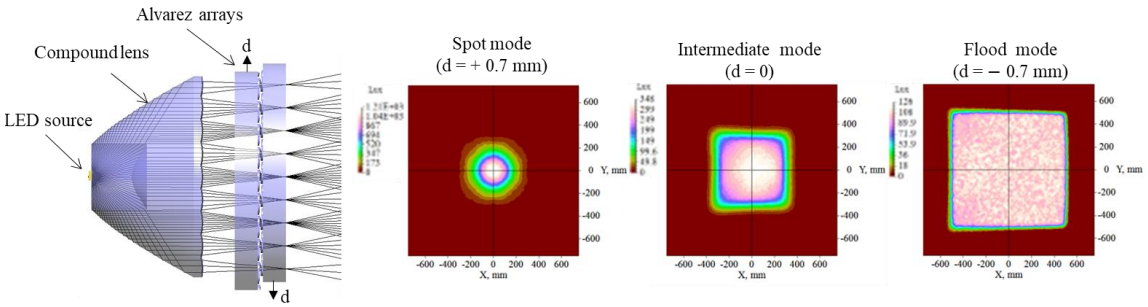

Fig. 3.1. The illuminance patterns of dynamic illuminator at three selected modes at 2 m distance, from Ref. [16].

In this paper, we adapt our previous design approach to realize a dynamic illumination system with high uniformity by combining a Lambertian LED source with commercial-off-the-shelf (COTS) optics and custom arrays of Alvarez lenses. Using the COTS elements in the design speeds up the process of building a demonstrator. Section 3.3 reviews the implementation and simulation results of the refined optical design, and Section 3.4 presents the optomechanical design and required manufacturing processes. Section 3.5 reviews the implementation of a camera-based test station to measure the illuminance of the demonstrator, along with test results and analysis of optical performance, followed by conclusions in Section 3.6.

3.3 Design realization

We previously reported on a design approach for dynamic illumination systems enabling continuous variable illumination from spot mode to uniform flood mode, as shown in Fig. 3.1 [16]. This illuminator consists of a Lambertian LED source, a custom compound lens including a total-internal-reflection (TIR) lens for collimating the light, a lens array for distributing the light into convergent ray bundles, and Alvarez arrays for

dynamically adjusting the size of the illumination pattern. In this section, this approach is adopted for a refined illumination system that utilizes COTS elements.

A COTS compound LED lens (KHATOD, PL1672) that combines a TIR lens with an integrated lens array was paired with a matching LED module (Centaurus Cree LED module by LUXdrive) which eliminates the soldering process of attaching the LED to the PC board and eases alignment challenges. The ‘static’ section of the design is constructed by attaching the compound lens to the LED module, as shown in Fig. 3.2. This static portion must be modeled before it can be used as a module in the dynamic illumination design. The default LightToolsTM source library was used to retrieve the optical model of this domed LED source (flux=100 Lumens, chip LED size 1.5 mm-by-1.5 mm). The size and radius of curvature (ROC) of each lenslet in the array are critical design parameters. The size of each lenslet was reported as 4 mm by 6 mm in the datasheet, but the optical form of the lenslets was not available from the vendor. As a consequence, an inverse engineering process was necessary, as described in [17]. The ROC was measured as 10.45±0.1 mm using scanning white-light interferometry.

Fig. 3.2. Constructing the static part of the tunable illuminator using the COTS optics.

The ‘dynamic’ section of the system, consisting of the transmissive Alvarez arrays, was also modeled in LightToolsTM with same unit size as the static lens array (4 mm-by-6

mm). The system was initiated and simultaneously optimized over spot and flood illumination modes. The collimated merit function was set for spot mode and a uniform rectangular-shape target merit function with an average Full-Width Half Max (FWHMAvg) of 1000 mm was set for the flood mode. The lenslet aperture shape defines the shape of the output light distribution, so the width-to-length ratio of the target pattern was set to the same value as the lenslets. The air gap between the Alvarez arrays was set at 0.5 mm. Additional polynomial terms were added to the basic Alvarez surface equations to minimize distortion defects in flood mode, as presented in [17]. The resulting surface equation for each element in the Alvarez array is given by:

$$z = 0.05\left(\frac{x^3}{3} + xy^2\right) + 0.019x^2 + 0.0241y^2 - 0.006x^2y^2 - 0.18x \qquad (3.1)$$

The final geometry of the dynamic illumination system is illustrated in Fig. 3.3 Simulated illuminance patterns (with 1,000,000 traced rays) for three chosen modes within the continuous variable illumination range are shown in Fig. 3.4. The transfer efficiency defined as the incident flux over the target plane to the total emitted flux from the LED source is about 96% without considering the Fresnel loss (~75% in present of Fresnel loss), which indicates a high-efficient design.

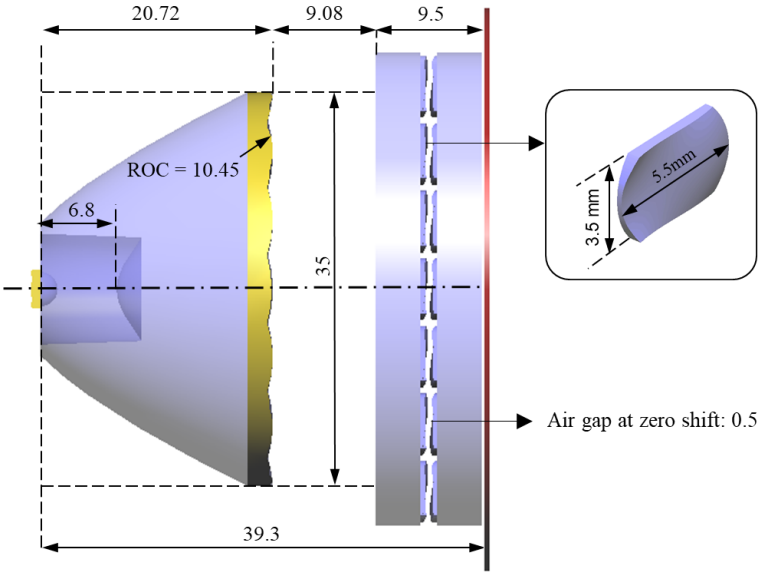

Fig. 3.3 The final geometry of the tunable LED-based illuminator (all units in mm).

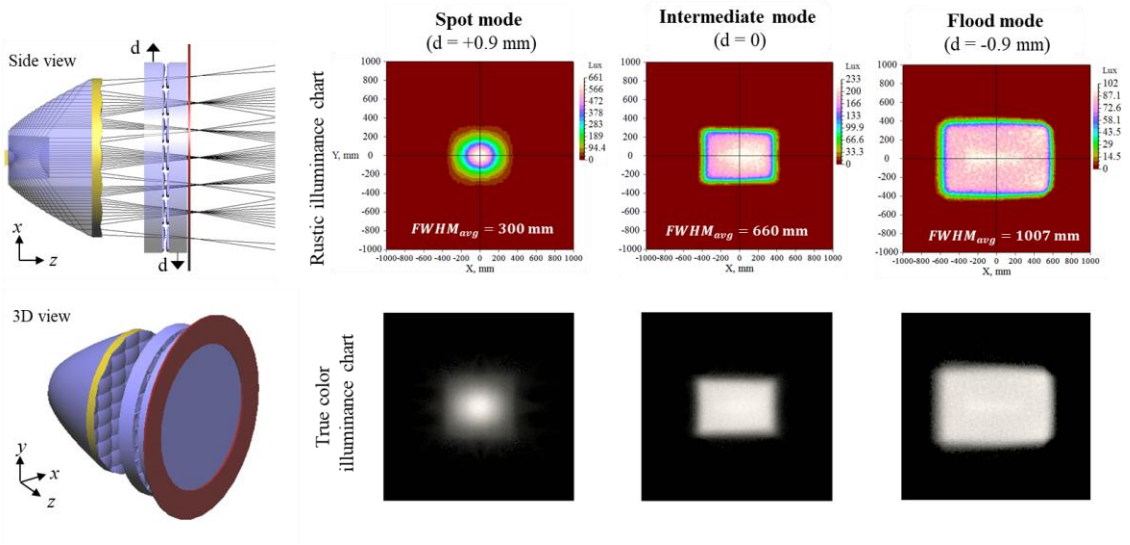

Fig. 3.4. Simulated illuminance patterns for spot, intermediate, and flood modes at 2 m from the source.

3.4 Optical and optomechanical fabrication

3.4.1 Optical system architecture

As discussed above, variable focal length of the Alvarez lenslet arrays is achieved by lateral relative translational movement between the freeform elements. While fully

translational sets of optics are the intended use case, the optomechanical system would utilize precision machined flexures or translational mounts, which can be time and resource intensive for sourcing or manufacturing. To expedite manufacturing and allow for more stable alignment and testing, we chose instead to manufacture three sets of Alvarez arrays with pre-set physical shifts (Fig. 3.5) in the surfaces corresponding to the desired illumination modes shown in Fig. 3.4.

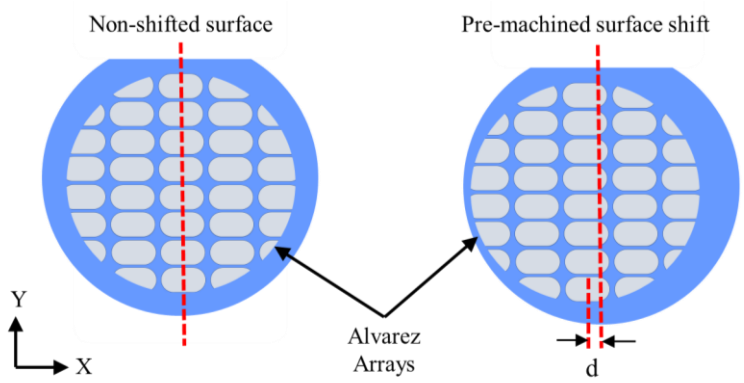

Fig. 3.5. Simplified image of shifting the optical surface, the combined shift table with a comparison of a finished Alvarez array.

The resulting optical system architecture, shown in Fig. 3.6, consists of one rear mounting plate, one optical barrel, the LED source, the COTS TIR lens, two steel alignment pins, four magnets (two for each mount), and the custom Alvarez arrays.

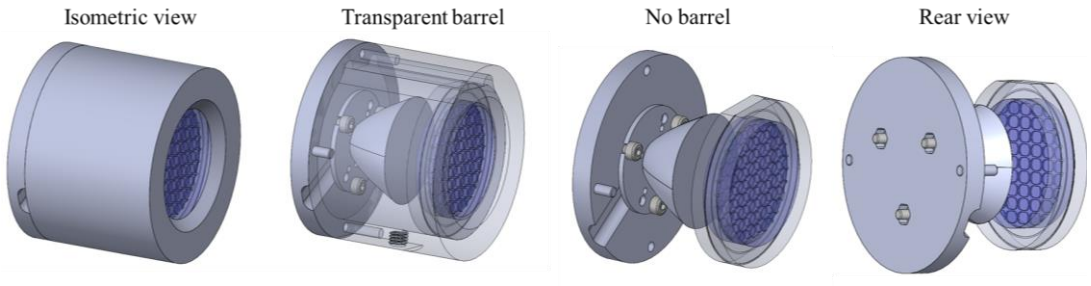

Fig. 3.6. Multiple views of CAD model for Alvarez array illumination system.

3.4.2 Manufacturing of optomechanical fixturing

The main goals for the optomechanical design were controlling spatial tolerances, reducing part count, and testing system compatibility. To these ends, the system was designed with a main housing consisting of one back mounting plate and an optical barrel to set the distances between the components. The plate and barrel were all machined from the same piece of aluminum (6061) bar stock with 63.5 mm outer diameter to facilitate tolerance and alignment preservation. The plate and barrel were each machined on the HAAS Computer Numerically Controlled (CNC) Toolroom mill (Fig. 3.7).

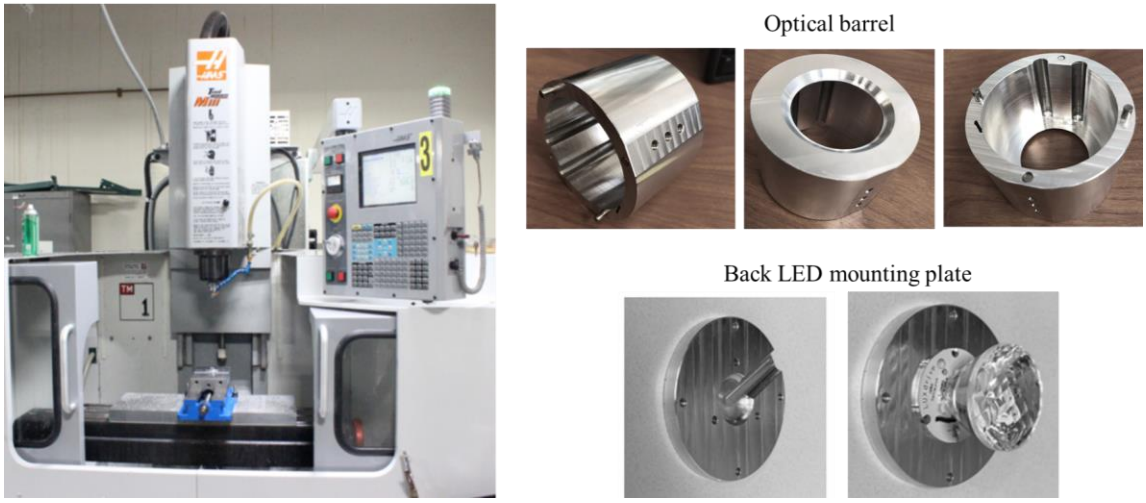

Fig. 3.7. A HAAS CNC Toolroom Mill with manufactured mountings.

One issue with the initial manufacturing of this mounting system was machining the center of the optical barrel. The overall length of the mounting is 51 mm, with the optical barrel bore at 41 mm deep. This bore's depth can lead to manufacturing problems like tool chatter and undercutting caused by tool deflection. To limit these issues the diameter of the milling tool was increased to 19.05 mm and tool shank relieved so it could reach full depth of cut without colliding with the barrel. A thin plastic spacer was designed, and 3D printed

to hold the optics in place in the optical barrel. Hardened steel machine pins with outer diameters of 3.175 mm and neodymium magnets were used to clock and hold the housings together for testing. Magnets were selected instead of fasteners (such as threaded rods or bolts) to avoid an over-constrained system. The magnets also simplify changing the Alvarez array components for the different illumination modes.

3.4.3 Optical Fabrication

Freeform surface manufacturing requires at least three axes of motion. The Alvarez arrays in our system were fabricated with a multi-axis ultraprecision diamond milling center with a 50,000 RPM milling spindle. Direct milling of the freeform surfaces was done using a diamond mill on three axes (X, Y, Z). While less common than a diamond turning of optical surfaces, diamond milling can enable the generation of surfaces with steeper slopes than are achievable with diamond turning with an optical surface finish [14, 18-20].

The freeform arrays were machined in two separate processes: (1) preparation of the optical blanks, and (2) ultraprecision diamond milling of the freeform optical surfaces. Initial blanking began with rough cutting of 50.8 mm diameter PMMA bar stock on a horizontal band saw into approximately 5 mm thick disks. These disks were then faced with a diamond tool with 1.008 mm tool nose radius on the Moore Nanotech 350FG using a 38.1 mm diameter aluminum vacuum chuck. The Moore Nanotech 350FG (Fig. 3.8), is a 5-axis precision diamond machining center with 3 linear axes (X, Y, Z) with 0.034 nm resolution and two rotary axes (B, C) with 1.75 nanoradian resolution. Total manufacturing volume on this machine is 350 mm by 150 mm by 300 mm (X, Y, Z). The machine is

enclosed in a temperature-controlled room at 20 C +/- 0.1 degrees C at 50% relative humidity to minimize thermal variations during manufacturing.

Fig. 3.8. Moore Nanotech 350FG is housed at UNC Charlotte in Duke Centennial Hall.

Once the rough-cut blanks have been faced on the front and back sides, the parts were milled on a HAAS Toolroom Mill using a jig to cut clocking flats for angular alignment of the parts. The outer diameters (OD) of the steel machine pins aligned with a circumscribed circle which matched with the optic's OD. This design enables an endmill with a known diameter to cut a flat on the outer diameter of the optical blank.

After the clocking flats were machined, the optical blanks were taken back to the Moore Nanotech 350FG for final freeform machining. Both faces of all optical blanks were diamond turned to ±1μm parallelism and the desired starting thickness. Three sets of Alvarez arrays, each set with the same form with the prescribed global surface shift, were then manufactured from the optical blanks using diamond milling on the Moore Nanotech 350FG.

Complex freeform toolpaths were generated using NanoCAM4®, a precision manufacturing software package which allows for the direct import of the surface equations and tooling parameters. The toolpaths were built by first importing the surface equation for a single Alvarez lenslet (Eq. 1 above) into NanoCAM4®. This singular lenslet surface was exported as a point cloud and compared to a MATLAB^{TM} generated interpolant map from the same prescription. This comparison showed no error between the two separately generated maps, validating that the optical surface in NanoCAM4® was correct. The validated lenslet surface in NanoCAM4® was then duplicated in the software to form an array. From that point, the milling tool was defined in the software and the toolpath was post-processed. The optical data within NanoCAM4® were offset by the required distances along the x-axis for each Alvarez array (-900, 0, or +900 μm, as shown in Figs. 3.4 and 3.5) and then the toolpaths were processed and exported for usage on the Moore Nanotech 350FG.

The optics were mounted for final surface cutting used a 10 PSI vacuum and a layout fluid. Layout fluid is a thin liquid, useful for mounting small parts on a vacuum chuck. When it dries, the layout fluid can act as a thin adhesive with no adverse effects on PMMA, unlike some other glues. The optical blanks were clocked on the pre-milled flat to within ±1 μm. A diamond milling tool with a tool nose radius of 247 μm was used. Direct milling of the surface began with roughing passes at a 50 μm depth of cut with 50 mm/min feedrate, and 5μm data density. A single finish pass was performed at a 10 μm depth of cut, 10 mm/min feed rate, and 0.5 μm data density. The overall milling of the optics took 52 hours to complete from roughing to finish passes. We note that this cycle time is impractical for

volume manufacturing, but that the resulting plastic freeform elements are conducive to molding for larger quantities.

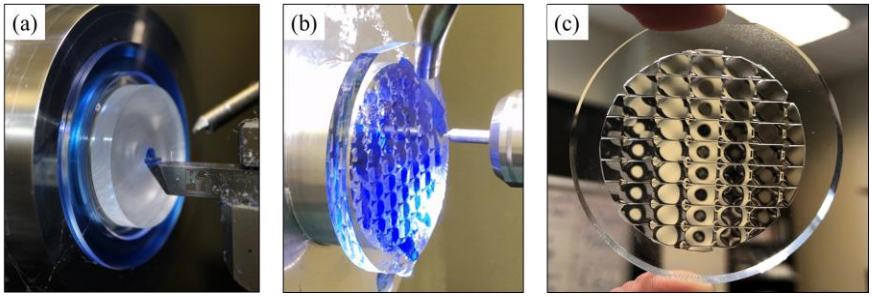

Fig. 3.9. (a) Diamond turning of surface to flat, (b) Diamond milling of the optical surface, (c) Final optic.

We were unable to measure the form of the resulting freeform optics at this time, but from prior experience we expect the form accuracy on the Moore Nanotech 350FG to be better than 0.10 µm Peak-to-Valley (PV) [21] Surface finish was measured using the ZYGO Zegage™ Plus 3D optical surface profiler (Fig. 3.10) on two separate Alvarez array plates. The optical surfaces were measured using 20x and 50x objectives with 3 averages and a Gaussian bandpass filter of 2.5 to 80 µm, following ISO 10110-8 [22]. These filters were chosen to isolate surface roughness from form and waviness. The average surface roughness (Sa) from measurements across the phase plate surfaces was 25 nm.

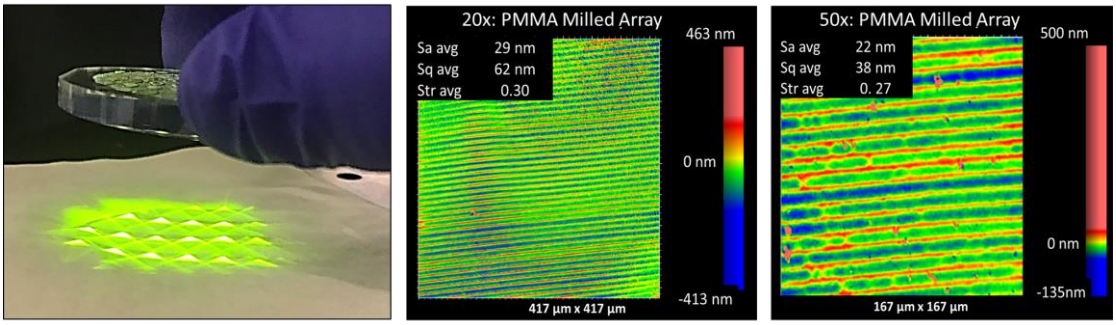

Fig. 3.10. Measurement of a finished Alvarez lenslet array and the average surface roughness measurements.

3.5 Performance characterization methods and results

3.5.1 Test system development and calibration

Optical performance analysis of an illumination system may be conducted using a variety of photometric quantities, including illuminance, intensity, and luminance. Illuminance is a good option for luminaires which defines the amount of luminous flux per unit area on a target plane (Lumen/m^2, or Lux) [23].

Measurement of illuminances value at selected test points over the target plane provides a general method for defining uniformity of illuminance pattern, with the grid size used to cover the test area varying according to different test standards [24]. This simple approach comes with potential disadvantage of missing information since the measurements are taken at discrete points on the target plane. The measurement process also can be time consuming if a luxmeter is used to measure the illuminance over the test points one-by-one. Another approach to characterize the illuminance pattern is capturing the light distribution projected on a diffused screen which provides a better understanding of the light distribution. However, commercially available calibrated test setups can be very costly. To address these issues, we developed a low-cost calibrated camera-based test station to characterize the illuminance pattern across a target plane. This test station includes a CMOS camera (FLIR BFS-U3-13y3M-C) with a 6 mm fixed-focal-length lens mounted on top of the dynamic illuminator. The monochromatic camera captured the light pattern projected on a diffusing screen set at 2 m distance, as shown in Fig. 3.11. A voltage stabilizer was connected to the LED source of the illuminator to regulate the input power since the emittance flux of the LED can fluctuate in response to changes in the input electrical voltage and current. The test experiments were performed at 700 mA operating

current with 3V running voltage. The test station was calibrated for both distortion and illuminance as described below.

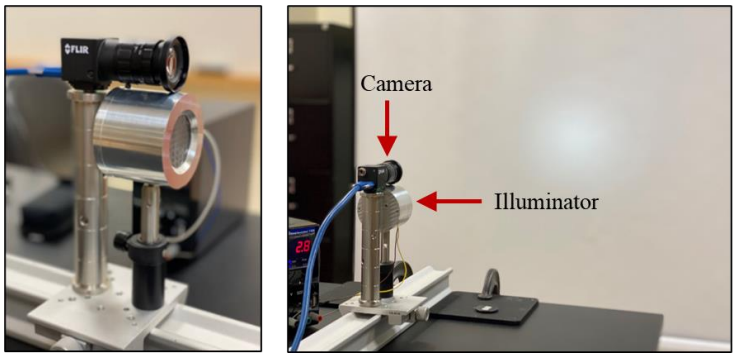

Fig. 3.11. Custom camera-based test station for illuminance measurement.

Distortion calibration was performed by estimating the geometrical parameters of the camera using the "Camera Calibrator" app in MATLAB™ [25]. As inputs, 20 different images of a standard checkerboard were captured by the CMOS camera at different locations and orientations. We used an adjustable monitor as a holder for positioning a printed checkerboard test sheet at different rotation and tilt angles. An image of the checkerboard before and after correction for camera lens distortion is shown in Fig. 3.12.

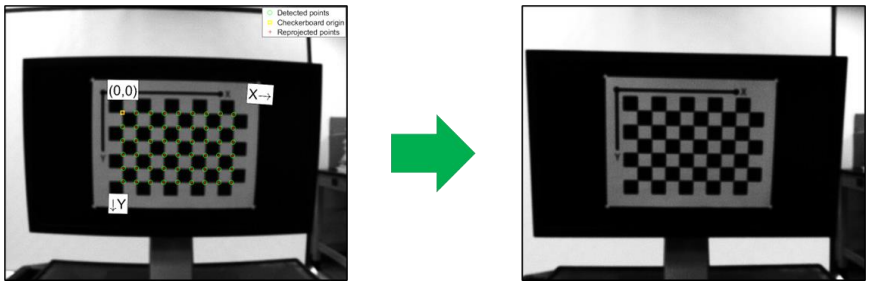

Fig. 3.12. Correcting camera lens distortion using the "Camera Calibrator" toolbox in MATLAB™

In next step, the illuminance was calibrated by comparing camera data with luxmeter data measured at selected test points in the light pattern generated from the static section of the illuminator (the LED and the compound TIR lens). First, as shown in Fig. 3.13, a

pattern with a grid of points on 10 cm spacing was attached to the screen and an image of it was recorded as a reference. Then, the illuminance values at the test points were measured with an LED light meter (LT45 EXTECH). The grid pattern was detached from the screen and multiple images of the light pattern were recorded with different camera gains and exposure times.

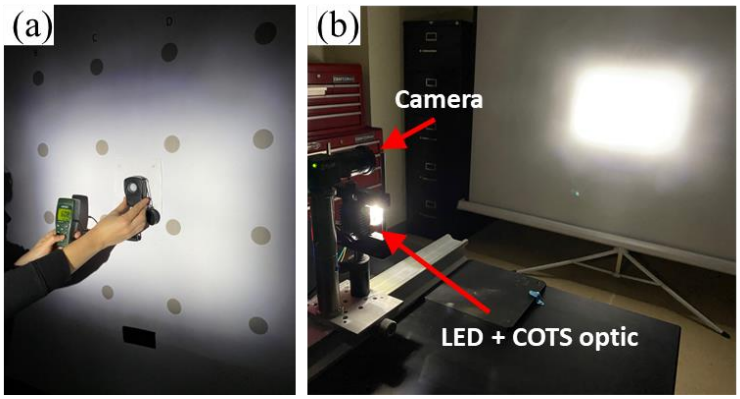

Fig. 3.13. Illuminance calibration process: (a) illuminance measurement by lux-meter, (b) capturing the light distribution by camera.

A custom code was developed in MATLAB™ to first correct for camera distortion as discussed above, and then crop the image to the desired size. The test point coordinates on the screen were then detected using image processing technique as shown in Fig. 3.14(a). The gray levels of the test points were extracted from the test images along with their coordinates. Linear regressions were performed to correlate the gray levels of the test points extracted from test images (between 0-255 for the 8-bit monochromatic camera) with the measured luxmeter data for the different camera settings. The camera setup with the minimum RMS error from the linear regressions was selected as the reference calibrated setup for subsequent measurements. The linear regression RMS error for the range of illuminance in this application (0 to ~ 650 Lux) is acceptable. This process was performed to simplify obtaining the response curve of the camera. The detail of the chosen

camera setup and the corresponding transfer function to correlate the image gray levels to the illuminance values are listed in Table 3.1. An illustration of the correlation between the camera image and luxmeter values for the chosen setup is shown in Fig. 3.14(b).

Table 3.1. Camera illuminance calibration and transfer function

Camera exposure time	Camera gain	Illuminance transfer function (Lux)	RMS error of linear regression (Lux)
100 mSec	0.96	3.1965 (image grey level) +7.04	6.78

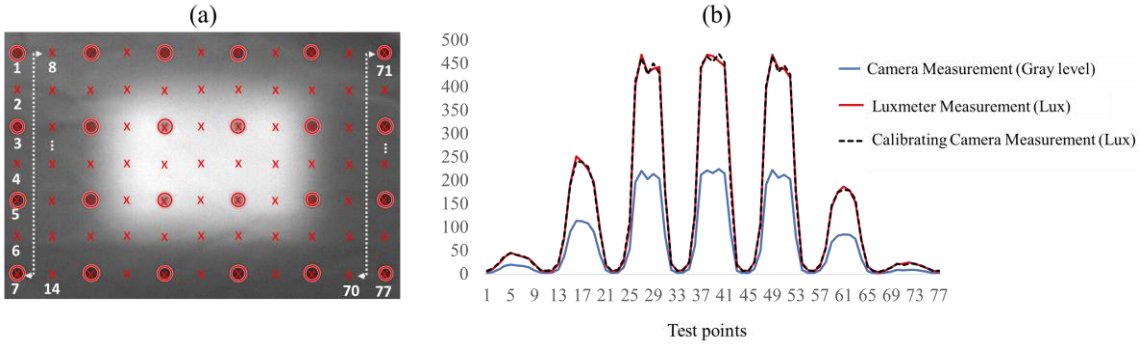

Fig. 3.14. (a) Detecting the test points on the test image to define their locations by using "imfindcircles", and (b) Correlating camera measurement to the luxmeter measurements using linear regression over test points.

3.5.2 Performance metrics and analysis software

We used two main performance metrics in this work to characterize the size and uniformity of the illuminance patterns: (1) The average full width at half of the maximum value of the light distribution ($FWHM_{avg}$) which is equal to the diameter of the circle with the same area as the area limited by FWHM; and (2) the Average Deviation (AD) as a statistical representation of illumination uniformity, defined as:

$$AD = \frac{1}{E_{avg}} \sqrt{\frac{1}{N} \sum_{i=1}^{N} [E(i) - E_{avg}]^2}, \qquad (1)$$

where E(i) is the illuminance value at each test point and E_{avg} is the illuminance average over all test points (N). We calculate AD over the area limited by $FWHM_{avg}$; zero AD corresponds to a perfectly uniform pattern.

MATLAB™ was used to create a standalone application to facilitate optical performance analysis. The graphical user interface (GUI) layout is shown in Fig. 3.15 for flood mode illumination as an example. The first column of the application connects to LightTools™ to upload simulation mesh results, and the user uploads the corresponding test image in the next column. Performance metrics to quantitatively characterize the illuminance patterns are then calculated automatically.

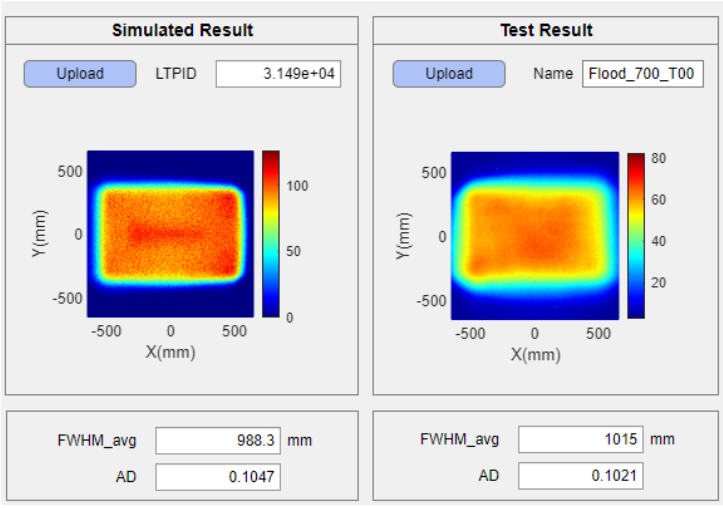

Fig. 3.15. Testing application to automate test post processing and compare the simulated and experimental results.

3.5.3 Testing results

The pairs of Alvarez arrays discussed in Section 3.3 were used to accommodate the spot, intermediate and flood modes. The images were captured using the CMOS camera settings from Section 3.5.1. The testing processes was repeated with a 2nd static part (LED +

compound TIR lens) to provide limited qualitative data on variability from LED binning and optomechanical alignment. Qualitative test images are shown in Fig. 3.16, and quantitative measurements of each mode using the MATLAB™ tools discussed in Section 3.5.2 are shown in Fig. 3.17.

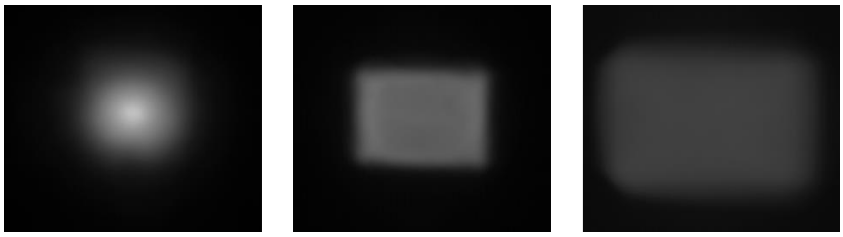

Fig. 3.16. Grayscale test images from the CMOS camera for the three selected illumination modes.

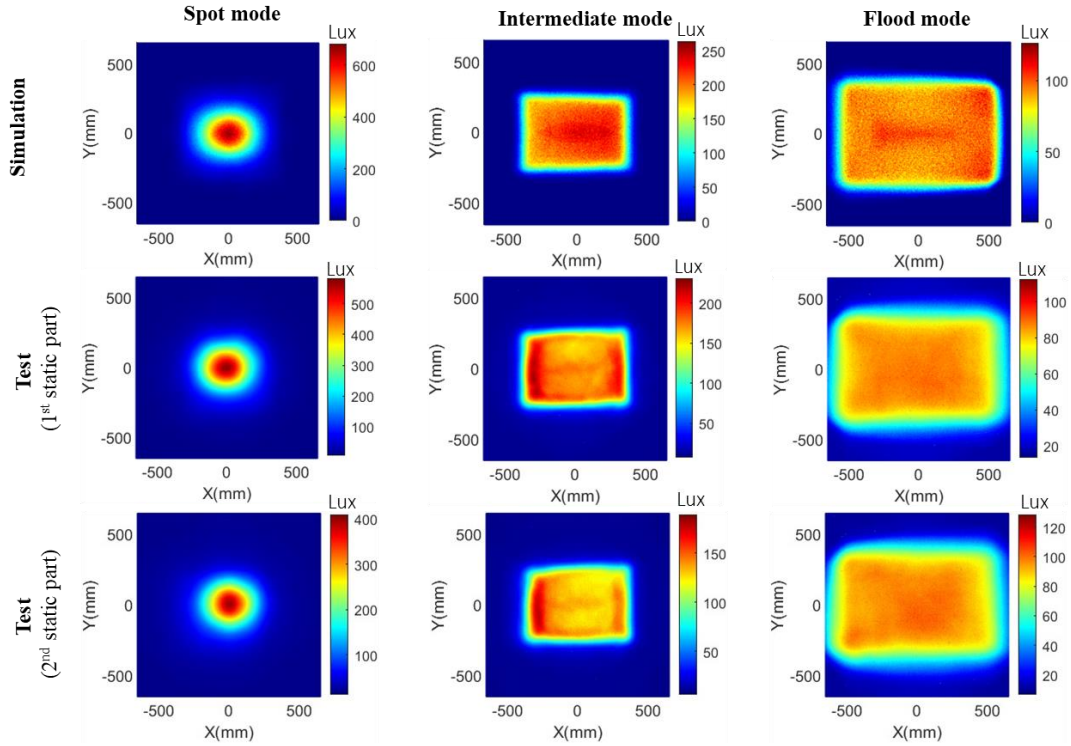

Fig. 3.17. Illuminance patterns of simulation and test results for three selected illumination mode from developed testing platform.

These experimental results demonstrate the dynamic illumination concept with good uniformity. Small differences between simulated and test results can be seen in Fig. 3.17,

which we believe result from surface scattering in the experimental parts and uncertainties in the simulations due to the need to estimate some geometrical parameters for the COTS TIR lens. Additional comparisons of performance metrics for these results are shown in Fig. 3.18.

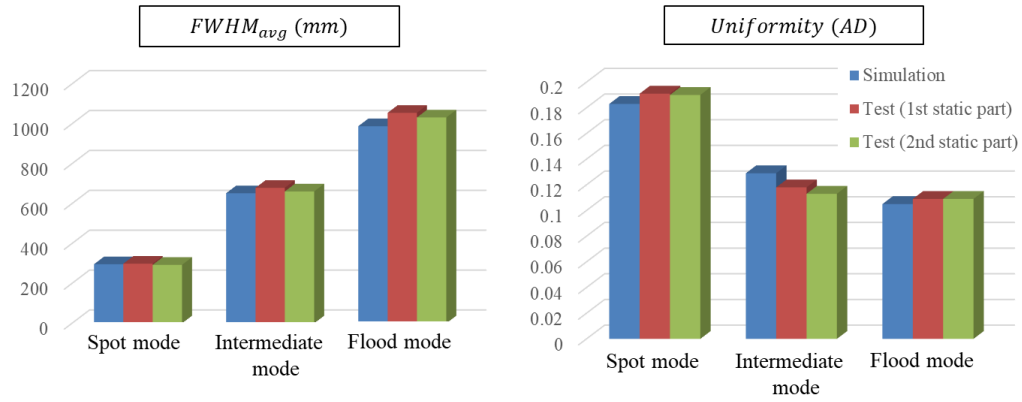

Fig. 3.18. Summary of performance metrics values for simulation and testing results.

3.6 Conclusion

We reported the design, manufacturing, and characterization of a tunable high-efficient LED-based illuminator to enable continuously variable light distributions from a spot mode to flood mode with high uniformity from non-uniform source through relatively small opposing lateral shifts applied to the freeform components. A commercially available optic was used in the design of a demonstrator to save costs and speed up the manufacturing process. To simplify the optomechanical design and proof of concept, a stationary housing holding switchable freeform arrays was built as an alternative to a continuously shiftable mechanism. Three sets of freeform arrays with pre-machined shifts corresponding to three selected modes of illumination were manufactured by Moore 350FG utilizing a diamond milling technique. The average surface roughness (Sa) of these freeform arrays was

measured 25 nm. A low-cost camera-based test station was also developed and calibrated to characterize the output illuminance pattern of illuminator across a target screen. In addition, a user-friendly application was developed to evaluate the optical performance of the demonstrator including pattern size and uniformity.

This study showed the test results of the built demonstrator for three chosen illumination modes. There were some discrepancies between the simulated and experimental results, which could be attributed to a number of things, such as inaccurate geometrical parameters determined for the COTS TIR compound lens model, optomechanical misalignments, and scattering problems. Nevertheless, the experimental results demonstrated and verified the dynamic illumination concept with good uniformity made possible by Alvarez arrays in an LED-based illuminator. In the future, it is advised to use mechanical or electrical actuators to provide the necessary shiftable mechanism of design.

3.7 References

1. A. J. Whang, S. Chao, C. Chen, Y. Chen, H. Hsiao, and X. Hu, “High uniform illumination of light-emitting diodes lighting with applying the multiple-curvature lens,” Opt. Rev. 18(2), 218-223 (2011).
2. J. M. Gee, J. Y. Tsao, and J. A. Simmons, "Prospects for LED lighting," Proc. SPIE 5187, 227-233 (2004).
3. W. S. Lee, “Zoomable LED flashlight,” U.S. patent 9,068,727 B2 (30 June 2015).
4. R. D. White and D.P. Weiss, “Lighting device with dynamic bulb position,” U.S. patent 4,339,788 (13 Jul. 1982).

5. J. B. Lee, B. I. Chiang, H. K. Ho, “Zoom spotlight using LED array,” U.S. patent 8,979,316 B2 (17 March 2015).
6. D. J. Stavely, " U.S. patent App. 2012/0121244 A1 (17 May 2012).
7. M. Bueeler and M. Aschwanden, “Illumination source with variable divergence,” U.S. patent 8,944,647 B2 (Feb 2015).
8. D. Y. Zhang, V. Lien, Y. Berdichevsky, J. Choi, and Y. H. Lo, “Fluidic adaptive lens with high focal length tunability,” Appl. Phys. Lett. 82(19), 3171-3172 (2003).
9. N. T. Nguyen, “Micro-optofluidic Lenses: A review,” Biomicrofluidics 4(3), 031501 (2010).
10. Z. Yongchao, “Development of solid tunable optics for ultra-miniature imaging systems,” Ph.D. dissertation (National University of Singapore, 2016).
11. G. Beadie, M. L. Sandrock, M. J. Wiggins, R. S. Shirk, M. Ponting, Y. Yang, T. Kazmierczak, A. Hiltner, and E. Baer, “Tunable polymer lens,” Opt. Express 16(16), 11847-11857 (2008).
12. P. Liebetraut, S. Petsch, W. Mönch, and H. Zappe, “Tunable solid-body elastomer lenses with electromagnetic actuation,” Appl. Optics 50(19), 3268-3274 (2011).
13. E. Savio, L. D. Chiffre, and R. Schmitt, “Metrology of freeform shaped parts,” CIRP annals 56(2), 810-835 (2007).
14. J. P. Rolland, M. A. Davies, T. J. Suleski, C. Evans, A. Bauer, J. C. Lambropoulos, and K. Falaggis, "Freeform optics for imaging," Optica 8, 161-176 (2021).
15. L. W. Alvarez and W. E. Humphrey, "Variable-power lens and system," U.S. patent 3,507,565A (21 April 1970).

16. S. Shadalou, W.J. Cassarly, and T.J. Suleski, "Tunable illumination for LED-based systems using refractive freeform arrays," Opt. Express 29(22), 35755-35764 (2021).
17. S. Shadalou, W.J. Cassarly, and T.J. Suleski, "Tunable LED-based illuminator using freeform arrays," Proc. SPIE 120780I (2021).
18. B. McCall, G. Birch, M. Descour, and T. Tkaczyk. "Fabrication of plastic microlens arrays for array microscopy by diamond milling techniques," Micromachining and Microfabrication Process Technology XV, Vol. 7590, 62-71. SPIE (2010).
19. F. Jiao and K. Cheng, "An experimental investigation on micro-milling of polymethyl methacrylate components with nanometric surface roughness," Proc. of the Ins. of Mech. Eng., Part B: Journal of Engineering Manufacture 228(5), 90-796 (2014).
20. K. P. Thompson and J. P. Rolland, "Freeform optical surfaces: a revolution in imaging optical design." Optics and Photonics News 23(6), 30-35 (2012).
21. Moore Nanotechology Systems, in Nanotech 350FG Specification Overview, Swanzey, NH (2007).
22. International Organization for Standardization, “Optics and photonics - Preparation of drawings for optical elements and systems - ISO10110-8” (2010).
23. R. J. Koshel, Illumination Engineering: design with nonimaging optics (John Wiley & Sons, 2012), Chap. 1.
24. D. J. Carter, R. C. Sexton, and M. S. Miller. "Field measurement of illuminance." Lighting Research & Technology 21.1 (1989): 29-35.
25. The MathWorks Inc. (R2020a), Camera Calibrator Toolbox, available at: www.mathworks.com/help/vision/ref/cameracalibrator-app.html

CHAPTER 4: A GENERAL DESIGN METHOD FOR DYNAMIC FREEFORM OPTICS WITH VARIABLE FUNCTIONALITY [82]

4.1 Abstract

We propose and demonstrate a general design method for refractive two-element systems enabling variable optical performance between two specified boundary conditions. Similar to the Alvarez lens, small, relative lateral shifts in opposite directions are applied to a pair of plano-freeform elements. The surface prescriptions of the boundary lenses and a maximum desired shift between freeform plates are the main design inputs. In contrast to previous approaches, this method is not limited to boundaries with similar optical functions, and can enable a wide range of challenging, dynamic functions for both imaging and non-imaging applications. Background theory and design processes are presented both for cases that are conducive to analytical surface descriptions, as well as for non-analytic surfaces that must be described numerically. Multiple examples are presented to demonstrate the flexibility of the proposed method.

4.2 Introduction

Modern optical systems benefit from freeform surfaces that enable compact and high-performance designs by utilizing additional design freedoms without the constraint of rotational symmetry [1]. Optical designs with continuously variable properties, or so-called dynamic optics, can add new, desirable functionalities for a wide range of both imaging and non-imaging applications, including cameras, aberration generators, microscopy, optometry, lighting, beam shaping, AR/VR, medicine/dermatology, and lithography [2-11].

Early examples of optical systems with multiple functions include bifocal single-element lenses used for spectacles and later designs of single-element lenses with gradually changing optical power using surfaces defined by involute curves [12-14]. While interesting and beneficial, single elements of this type use only a portion of the clear aperture for each function.

Liquid lenses are another way to offer flexible functionality to an optical system by modulating lens curvature or refractive index. [15-21]. However, liquid lenses have potential drawbacks such as leakage, evaporation, manufacturing complexity, and performance instabilities. While zoom lens systems have been reported to enable continuously variable optical power and dynamic beam shaping [22-24], such systems usually involve multiple optics and require longitudinal movement of the components, which can result in larger system sizes.

Another type of dynamic lens system employs refractive lens pairs capable of generating continuously variable optical power by applying shifts in a transverse plane with respect to the optical axis. Early designs were based on the direct superposition concept in which the output wavefront can be considered as a superposition of individual wavefront deformations due to passing through each individual refractive plate. Examples using this approach generate adjustable optical power with two orthogonally shifted cylinder lenses with varying radii of curvature [25-27]. The individual elements were constructed as segments of a cone or involutes of a circle. This approach introduces distortion due to non-uniform optical power across the clear aperture and requires large lateral shifts that are undesirable in compact optical systems.

The next generation of dynamic optics was enabled using an integral method with pairs of plano-freeform refractive elements. By applying lateral relative shifts in opposite directions to freeform pairs with matching surfaces, the output wavefront deformation can be related to the derivative of the individual freeform surfaces and the amount of applied shift [2, 3, 7, 28]. Compared to the direct superposition approach described previously, the integration approach requires significantly smaller lateral shifts without introducing significant distortion. The Alvarez lens system is a well-known example of this approach that enables continuously tunable optical power [2]. Palusinski later extended the Alvarez concept to enable variable aberration generators [7]. The general form of these systems has a symmetrical working range with zero optical power P at no shift ($a = 0$) and inverse optical power at the same shifts in positive and negative directions, as shown in Fig. 4.1.

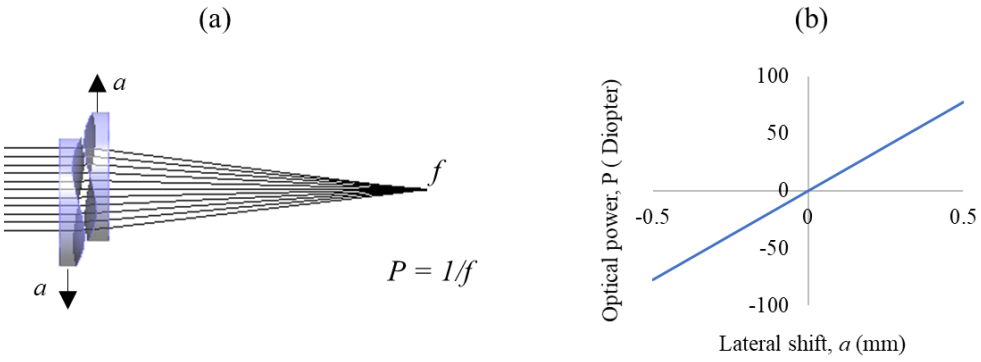

Fig. 4.1. (a) Schematic illustration of Alvarez lens system operation, (b) Optical power P vs. lateral shift for a sample Alvarez lens system.

Researchers later proposed a simple design adjustment to shift the working range of the Alvarez lens to break the symmetric constraint and enable optical power at zero relative shift ($a = 0$) [29]. However, breaking the symmetric constraint becomes more difficult when other dynamic optical properties are considered. Researchers recently reported dynamic beam shaping elements based on the Alvarez concept that transform a Gaussian

input beam into uniform irradiance outputs of different sizes with optical power at zero relative shift [30-33]. Although the reported results are very promising, the method requires multiple intermediate static designs and curve fits that can be time-consuming, and the target size is assumed to change linearly with lateral shifts of the freeform plates, which may not always be the case. Defining target patterns in advance is challenging for cases having non-linear relations between shift and target size.

Previous design approaches for dynamic freeform optics have also been limited to optical composites with similar functions along the shifting range of the freeform elements. For example, the Alvarez lens enables variable spherical power, and adjustable aberration generators vary a specific aberration along the working range. In contrast, consider an optical system working between non-similar optical conditions, such as a novel beam-shaping system capable of dynamically changing the output from a circle to a square. In addition, modern non-imaging designs can heavily utilize freeform surfaces obtained by numerical design approaches for compact, efficient optical systems [34-46]. The resulting surfaces are usually described by point clouds rather than equations. Variable illumination modes have been previously enabled by switching optical components [47, 48]; However, designing dynamic systems to enable continuously variable optical performance for these types of systems is challenging and not been addressed by previous design methods.

In this paper, we extrapolate the previously reported approach for dynamic beam shaping [30-33] to form a generalized design method capable of varying optical performance between two arbitrary boundary conditions. This method eliminates the needs for intermediate designs and symmetrical constraints in the working range required by previous approaches. In addition, this method can be applied to surfaces described

analytically by equations or numerically through point clouds. The resulting designs can be used directly in optical systems or considered as starting points for further optimizations using optical software based on the required accuracy and performance. The proposed method enables novel optical concepts for both imaging and non-imaging applications.

Section 4.3 presents a detailed overview of the proposed design method. Sections 4.4 and 4.5 demonstrate and verify the general design method with simulation results for both analytical and numerical design examples, followed by conclusions in Section 4.6.

4.3 General design method for dynamic freeform optics

The proposed general technique combines the superposition and integration approaches outlined in Section 4.2 to speed up and facilitate complex designs. Thin lens approximations and no air gap between the freeform pairs are assumed in theory. The optical material is the same for both boundary elements and the resulting freeform plates, but different materials may be used if the respective refractive indices are considered. To simplify the calculations, the thickness variation parameter illustrated in Fig. 4.2 as *T(x, y)*, has been used [7].

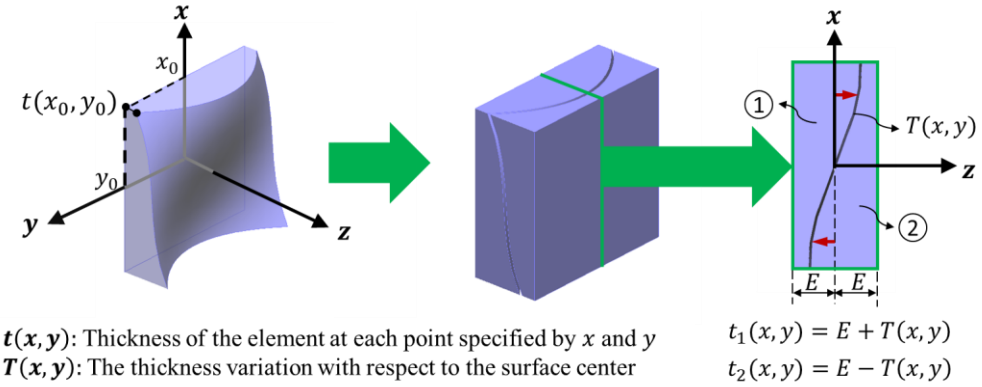

Fig. 4.2. Illustrating the geometrical thickness and thickness variation of a double refractive element.

The key inputs for the proposed method are two static designs representing the performance boundaries, and the maximum lateral shift value (a_{max}) between the freeform pairs. The integration technique can be used to construct a dynamic system with plano-freeform plates if static boundary elements have inverse optical thicknesses. As presented by Palusinski *et al.* in [7], the optical path difference concept can be used to calculate the wavefront deformation of a collimated beam passing through the shifting plates. The same notation is used here to avoid confusion. The optical path difference imposed by each plate is:

$$OPD(x, y) = (n-1)T(x, y), \tag{4.1}$$

where n is the refractive index, $T(x, y)$ is the thicknesses variation, and x and y are transverse coordinates across the plane perpendicular to the optical axis, as shown in Fig. 4.2.

When two lenses with inverse optical thicknesses are each laterally displaced by distance a in opposite directions along the x axis, as shown in Fig. 4.3, the resulting wavefront deformation is given by

$$W(x, y) = (n-1)[T(x+a, y) - T(x-a, y)]. \tag{4.2}$$

The wavefront deformation can be rewritten and simplified as follows:

$$W(x, y) = 2a(n-1)\frac{[T(x+a, y) - T(x-a, y)]}{2a} \approx 2a(n-1)\frac{\partial T(x, y)}{\partial x}. \tag{4.3}$$

The effective composite optical thickness of the two plates is thus given by

$$T_C(x, y) \approx 2a\frac{\partial T(x, y)}{\partial x}. \tag{4.4}$$

Eq. (4.4) relates the composite optical thickness of two refractive plates with inverse surfaces to the relative lateral shifts between them and the derivative of the optical thickness variation. For design, the inverse problem starts from the composite optical thicknesses with maximum shift values applied and derives through integration the

required optical thicknesses of the freeform elements needed for dynamic functionality. In the case of the simple Alvarez lens, then the composite thickness is $2\beta a(x^2+y^2)$ and the thickness variation is β ($x^3/3+xy^2$). A tilt term can be added to the thickness variation as $\beta(x^3/3+xy^2)+Dx$, where D is weighting coefficient, to minimize the thickness of the freeform plates without impacting the calculations [2, 7].

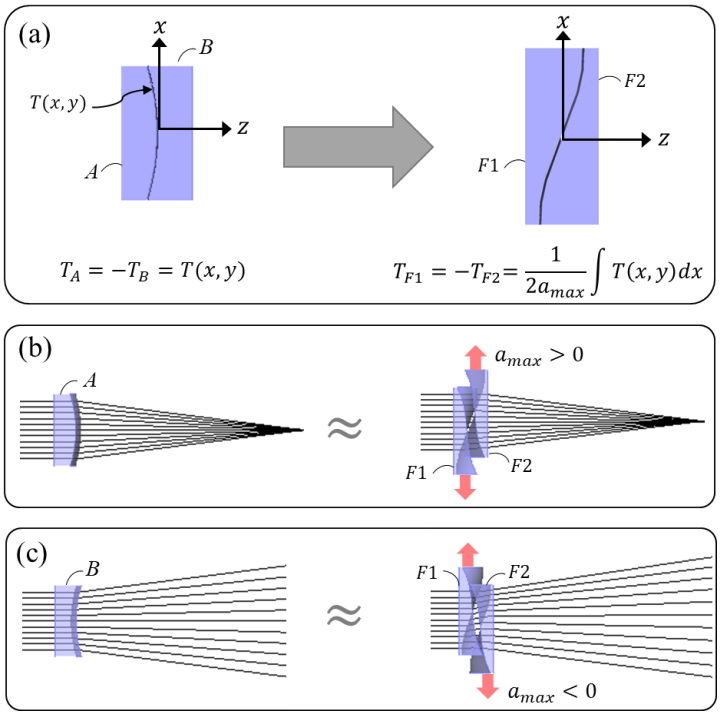

Fig. 4.3. (a) Design of dynamic freeforms from boundary elements with inverse thickness variation. For an example Alvarez lens, ray tracing through (b) first boundary element and dynamic system at maximum positive shift, and (c) second boundary element and dynamic system as maximum negative shift.

The design approach described in [30-33] for dynamic beam shaping considers cases in which the two boundaries do not have matching thicknesses but do have comparable functions and surface prescriptions, and identifying intermediate static designs is possible. In this paper we generalize existing methodologies to enable rapid dynamic designs that work between two arbitrary optical conditions without the need for intermediate static designs.

To derive general formulas for dynamic freeform pairs, we first consider thickness variations of two boundary elements $T_A(x, y)$ and $T_B(x, y)$ with no matching constraints. These two boundaries are transformed into two intermediate elements using the average thickness variation, as illustrated in Fig. 4.4. The thicknesses variation of the new elements, $T_{A'}(x, y)$ and $T_{B'}(x, y)$, are then calculated as follows:

$$T_{A'} = T_A - T_{avg} = T_A - \frac{(T_A + T_B)}{2} = + \frac{(T_A - T_B)}{2}, \tag{4.5}$$

$$T_{B'} = T_B - T_{avg} = T_B - \frac{(T_A + T_B)}{2} = - \frac{(T_A - T_B)}{2}. \tag{4.6}$$

Eqs. (4.5, 4.6) show that the 'new' boundary elements have inverse thickness variations, and thus the design problem can be solved using the integration approach discussed previously. Thus, variable optical properties changing from $T_{A'}$ to $T_{B'}$ are achieved as opposite lateral shifts are applied to a pair of freeform plates with the following optical thicknesses:

$$T_{F1'} = -T_{F2'} = \frac{1}{2a_{\max}} \int T_{A'} dx = \frac{1}{2a_{\max}} \int \frac{T_A - T_B}{2} dx, \tag{4.7}$$

where a_{max} is the magnitude of the maximum lateral shift applied to each dynamic plate in opposite directions.

Finally, to transform back to the original design problem varying from $T_A(x, y)$ to $T_B(x, y)$, the superposition concept is applied to add the initially extracted average optical thickness back to the system. Therefore, the final optical thicknesses of the dynamic freeform plates are given as follows:

$$T_{F1} = T_{F1'} + \frac{T_{avg}}{2} + Dx = + \frac{1}{2a_{\max}} \int \frac{T_A - T_B}{2} dx + \frac{T_A + T_B}{4} + Dx, \tag{4.8}$$

$$T_{F2} = T_{F2'} + \frac{T_{avg}}{2} - Dx = -\frac{1}{2a_{\max}} \int \frac{T_A - T_B}{2} dx + \frac{T_A + T_B}{4} - Dx, \tag{4.9}$$

where the *Dx* tilt term is added to minimize the thicknesses of the dynamic freeform plates. The overall design process is illustrated graphically in Fig. 4.4.

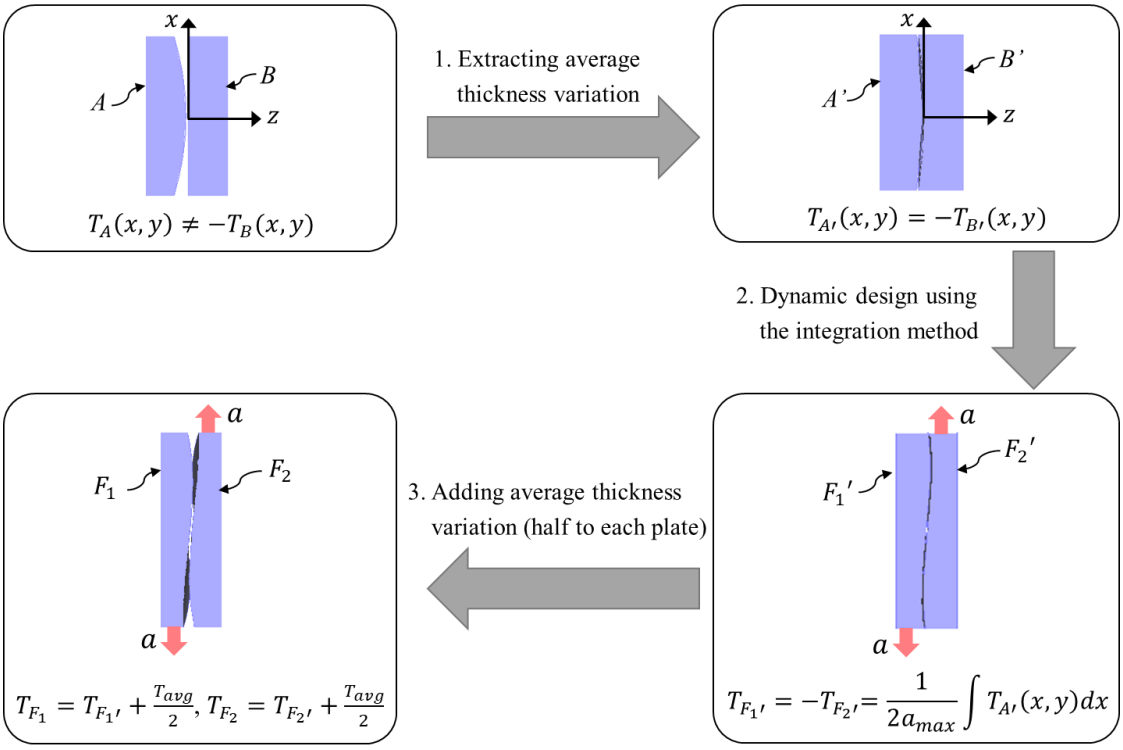

Fig. 4.4. Moving from arbitrary static boundary designs to dynamic dual element system using proposed method.

As a test, we apply the maximum shift a_{max} to the dynamic freeform plates and check the output wavefront as a superposition of wavefront deformations induced by each plate:

$$W(x,y) = (n-1)[T_{F1}(x + a_{\max}, y) + T_{F2}(x - a_{\max}, y)]$$

$$= (n-1)\left[\frac{1}{2a_{\max}}\int \frac{T_A(x + a_{\max}, y) - T_B(x + a_{\max}, y)}{2} dx + \frac{T_A(x + a_{\max}, y) + T_B(x + a_{\max}, y)}{4}\right.$$

$$\left. - \frac{1}{2a_{\max}}\int \frac{T_A(x - a_{\max}, y) - T_B(x - a_{\max}, y)}{2} dx + \frac{T_A(x - a_{\max}, y) + T_B(x - a_{\max}, y)}{4}\right]$$

$$= (n-1)\left[\frac{1}{2}\int \frac{T_A(x + a_{\max}, y) - T_A(x - a_{\max}, y)}{2a} dx - \frac{1}{2}\int \frac{T_B(x + a_{\max}, y) - T_B(x - a_{\max}, y)}{2a} dx\right.$$

$$\left. + \frac{T_A(x + a_{\max}, y) + T_A(x - a_{\max}, y)}{4} + \frac{T_B(x + a_{\max}, y) + T_B(x - a_{\max}, y)}{4}\right]$$

$$\approx (n-1)\left[\frac{T_A(x,y)}{2} - \frac{T_B(x,y)}{2} + \frac{T_A(x,y)}{2} + \frac{T_B(x,y)}{2}\right] \approx (n-1)T_A(x,y) \approx W_A(x,y). \qquad (4.10)$$

Thus, within the assumed approximations of thin-phase and zero-air gap, a maximum relative shift in one direction creates the wavefront deformation of the first optical boundary condition, $W_A(x, y)$. Analogous calculations for the maximum shift in the opposite direction creates the wavefront deformation of the second optical boundary condition, $W_B(x, y)$.

While determining the exact error and optimizing the dynamic system for non-zero thickness is more involved, optical design software can be used for further optimization to minimize the errors based on the accuracy required in various applications. Similarly, the physical distance between dynamic freeform pairs was neglected to simplify the calculations. To decrease this air gap in real designs and to simplify optic manufacturing by lowering the surface depth modulation, it is recommended to include a tilt factor in both freeform surfaces as discussed previously. We note that the proposed design method may produce equivalent or dissimilar freeform plates depending on the two boundary designs as presented in Eqs. (4.8, 4.9). Finding a tilt factor that minimizes the sag is straightforward in the case of identical plates, but we recommend choosing a tilt factor that minimizes both surface depth modulations concurrently for dissimilar plates.

While the processes and derivations discussed above are analytical in nature, the proposed design methodology can be implemented either analytically or numerically. The analytical approach is the logical choice if the boundary elements are readily defined by surface equations that can be integrated analytically. However, if the boundary elements are produced numerically and specified in point clouds, a numerical implementation of the same procedures is desirable alternative since it eliminates the need for curve fitting the surfaces of the boundary elements. Numerical methods are also advantageous when boundary surface equations are provided but the integration of their difference is challenging or the acquired solution for the dynamic plates is difficult to create analytically in optical software. However, further optimization of numerical freeform surfaces may be more difficult. Both analytical and numerical implementations are discussed and demonstrated in greater detail in the following sections using multiple design examples.

4.4 Analytical design examples for dynamic freeform optics

In this section, the analytical implementation of the proposed general design method is demonstrated through several examples. We assumed that the boundary elements and their corresponding dynamic freeforms are constructed of identical materials. After definition of the design parameters and boundary elements for each example, the thickness variations for the dynamic freeform plates are computed using the method of Section 4.3. The thickness variations can be related to surface profiles to model the optical elements in optical software. To ease the manufacturing process and allow for smaller air gaps between freeform plates, the surface modulations are reduced by applying the same linear tilt factor to each of the freeform surface equations. To ensure the same clear aperture as the boundary

elements in a dynamic system, an additional section equal to the overall shift range must be added to each freeform plate, as illustrated in Fig. 4.5.

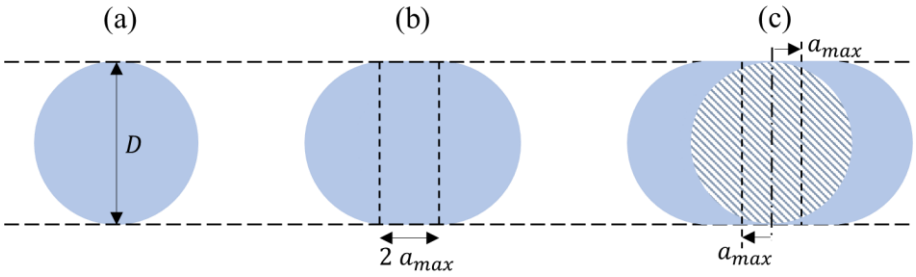

Fig. 4.5. (a) Aperture geometry of a circular boundary element, and (b, c) corresponding aperture geometry of resulting dynamic plates.

The first example demonstrates variable positive spherical optical power, the second illustrates variable cylindrical power, and the final example generates a uniform circular irradiance pattern from a Gaussian He-Ne laser and smoothly converts it to a uniform square-shaped irradiance pattern. As discussed previously, the proposed method requires two static boundary designs and the maximum lateral shift of dynamic freeform plates as the main inputs. The design process and simulation results are presented for each example. The first two cases are simulated in LightTools™ and the third is evaluated in VirtualLab Fusion™.

4.4.1 Analytical Example 1: Variable positive-spherical power lens system

For this example, we assumed polycarbonate as the design material and a 550 nm design wavelength. The boundary elements have circular apertures with 4 mm diameters and 0.75 mm thicknesses. Unlike the traditional Alvarez lens, this design has positive power at a = 0 and for all values. Table 4. 1. lists the input parameters and the resulting

freeform surfaces calculated using Eqs. (4.8, 4.9). The linear tilt term in the freeform plates is calculated using MATLAB ™ to minimize the overall sag along the freeform surfaces.

Table 4. 1. Primary inputs and outputs of variable positive-power lens system example

Main inputs	First boundary element	Flat with zero optical power, $T_A(x, y)=0$, $P_A = 0$
	Second boundary element	$T_B(x, y) = -0.05(x^2 + y^2)$, $P_B = 61$ *Diopter*
	Lateral shift range	$-0.4 < a < +0.4$ *mm*
Main outputs	First freeform plate	$T_{F1}(x, y) = 0.03125(\frac{x^3}{3} + xy^2) - 0.0125(x^2 + y^2) - 0.0743x$
	Second freeform plate	$T_{F2}(x, y) = -0.03125(\frac{x^3}{3} + xy^2) - 0.0125(x^2 + y^2) + 0.0743x$

The boundary lenses and resulting dynamic design were modeled using LightTools™, as illustrated in Fig. 4.6. A 100 µm air gap was set between the freeform plates to ensure that they do not contact during shifting. The dynamic freeform pair delivers variable positive optical power (and focal length) between the boundary values, as shown in Fig. 4.7 and Visualization 4.1.

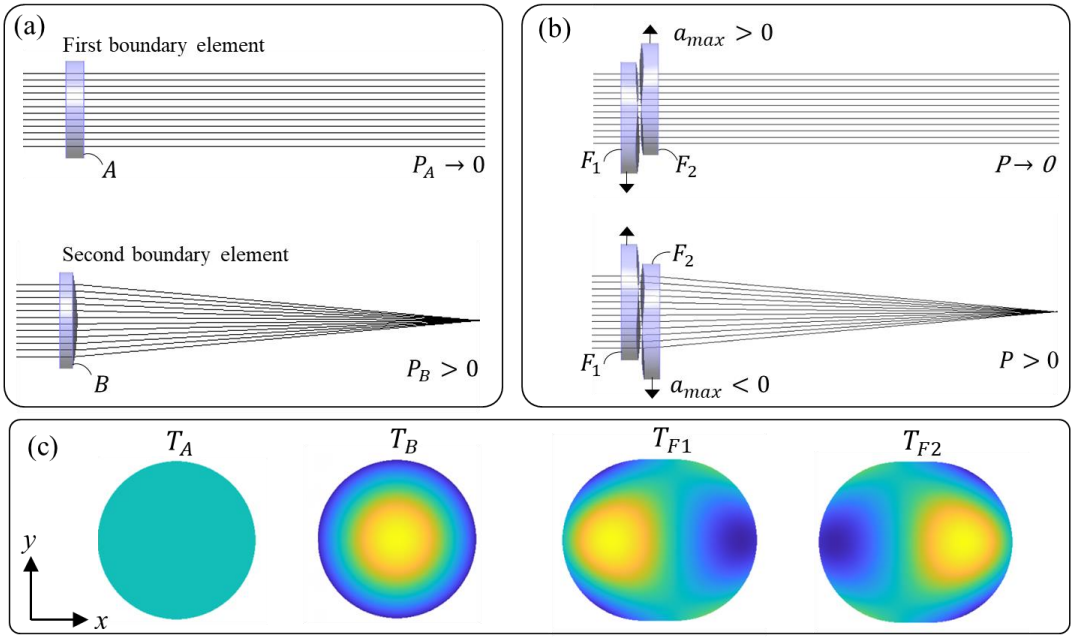

Fig. 4.6. Ray traces for (a) boundary elements vs. (b) dynamic freeform plates with maximum lateral shifts applied for first design example, and (c) thickness variations of boundary and dynamic freeform elements.

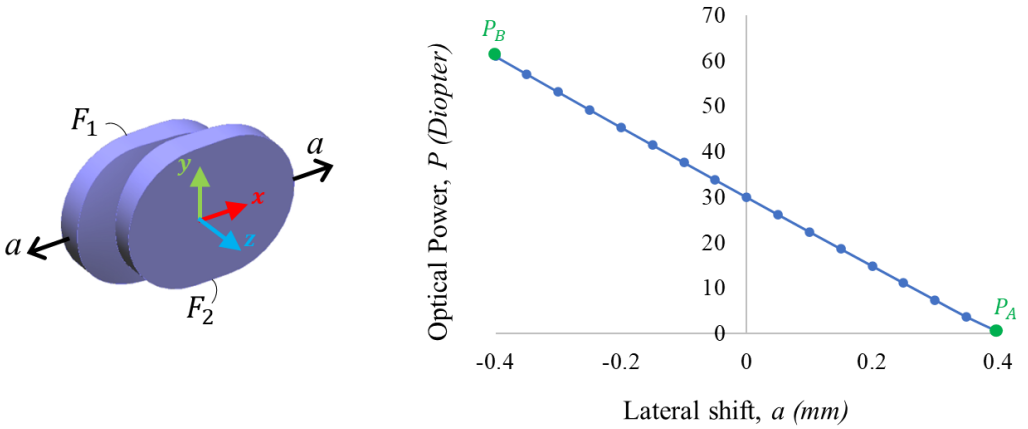

Fig. 4.7. Optical power vs. lateral shift for variable positive-power lens system.

4. 4. 2 Analytical Example 2: Variable cylindrical lens system

The second design example demonstrates a variable cylindrical lens system using the proposed design method. The same general configuration and design parameters as in the first example are used here, but with different boundary element surface equations and dynamic freeform shift range, as shown in Table 4.2. As before, the equations of the dynamic freeform surfaces are calculated using Eqs. (4.8, 4.9) and a linear tilt term added to reduce the depth modulation.

Table 4.2. Primary inputs and outputs of variable cylindrical lens system example.

Main inputs	First boundary element	$T_A(x,y) = -0.04x^2$
	Second boundary element	$T_B(x,y) = -0.04y^2$
	Lateral shift range	$-0.5 < a < +0.5$ mm
Main outputs	First freeform plate	$T_{F1}(x,y) = +0.02(xy^2 - \frac{x^3}{3}) - 0.01(x^2+y^2) + 0.0084x$
	Second freeform plate	$T_{F2}(x,y) = -0.02(xy^2 - \frac{x^3}{3}) - 0.01(x^2+y^2) - 0.0084x$

LightTools^{TM} was again used to model boundary elements irradiated by a uniform disc source with a diameter of 3 mm. Fig. 4.8 shows the output irradiances of the simulated

boundary elements at 1 m distance. Fig. 4.9 and Visualization 4.2 illustrate the optical performance with various shifts between the boundaries.

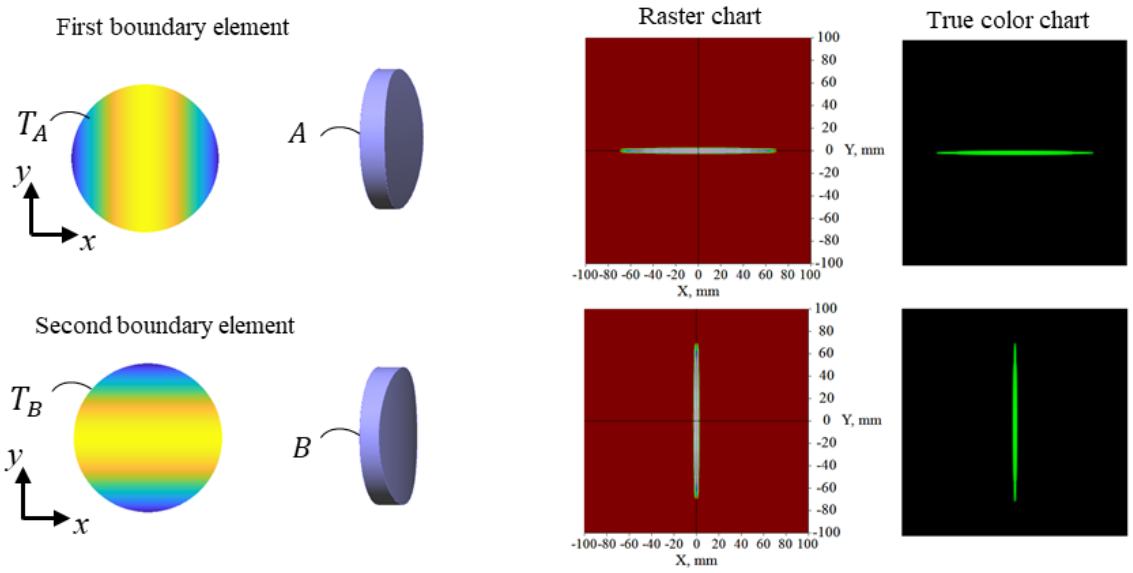

Fig. 4. 8. Irradiance patterns at 1m distance from a uniform collimated disc source after the boundary elements.

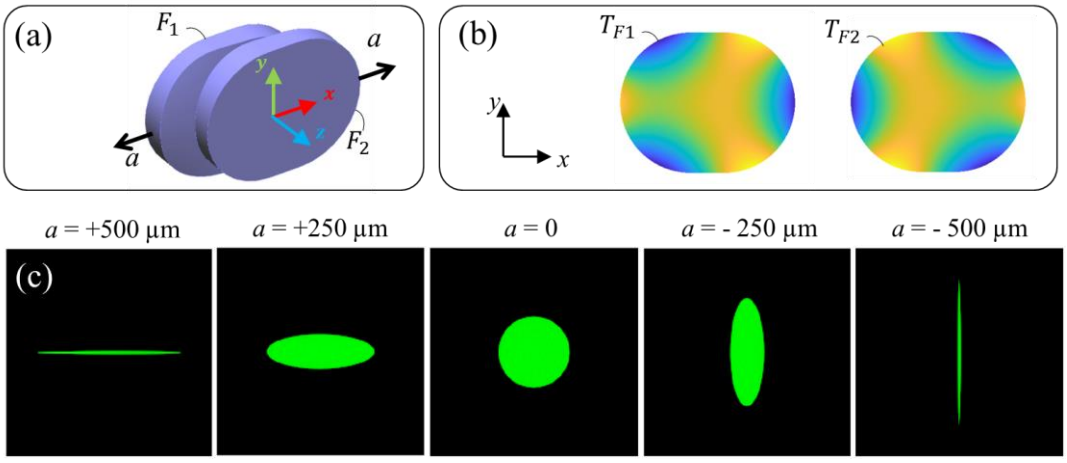

Fig. 4.9. (a, b) Freeform surfaces, and (c) irradiance patterns at 1m distance from a uniform collimated disc source after passing the tunable cylindrical-power lens system at different lateral shifts.

4.4.3 Analytical Example 3: Circular to square dynamic beam shaper

This design example develops a dynamic beam shaper that converts a circular Gaussian input beam from a uniform circular output pattern to a uniform square output pattern. Static designs of circular and square beam shapers presented in [39] were used to accelerate the design process. As illustrated in Fig. 4.10, the first boundary element produces a uniform circular distribution, and the second boundary element delivers a square shape of irradiance output from a Gaussian incident beam. Table 4.3 lists the design parameters. The analytical design equations for each boundary element are presented in Supplement 4.1.

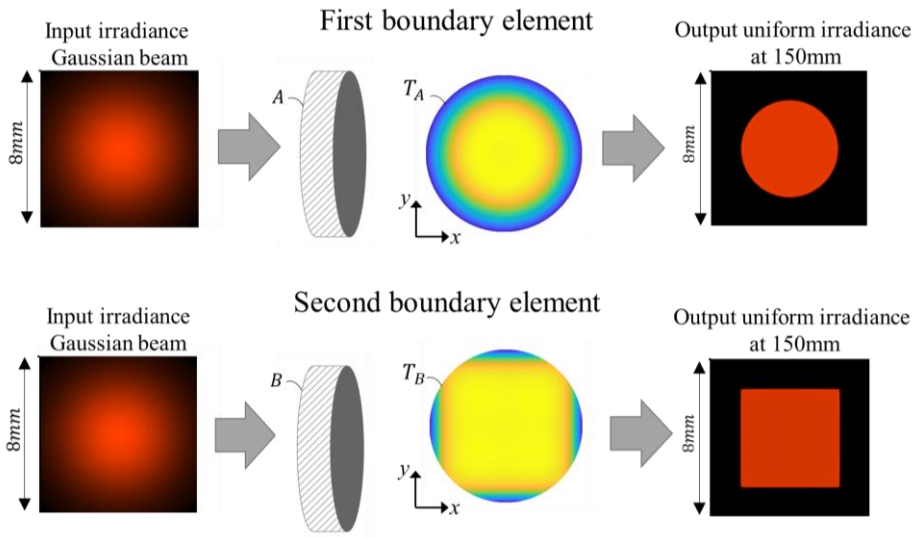

Fig. 4.10. Boundary elements of 3rd design example.

Table 4. 3. Input design parameters for dynamic beam shaper example

Wavelength	632.8 nm
Input beam waist diameter	6 mm
Material (index)	PMMA (n =1.49)
Target distance	150 mm
Boundary element diameters	12 mm
Boundary element thicknesses	2 mm
First boundary output beam diameter	5 mm
Second boundary output beam square side	5 mm
Lateral shift range of freeform pair	-300 < *a* < +300 μm

As before, the surface profiles of the dynamic freeform plates are computed by Eqs. (4.8, 4.9) using the boundary element profiles and maximum shift range. The resulting freeform surface equations are presented in Supplement C. The resulting coefficients were then used to model the dynamic freeform system in VirtualLab Fusion^{TM}. as shown in Fig. 4.11. The surfaces in this design example are much more complex than the first two cases, illustrating the power and flexibility of the proposed general design method.

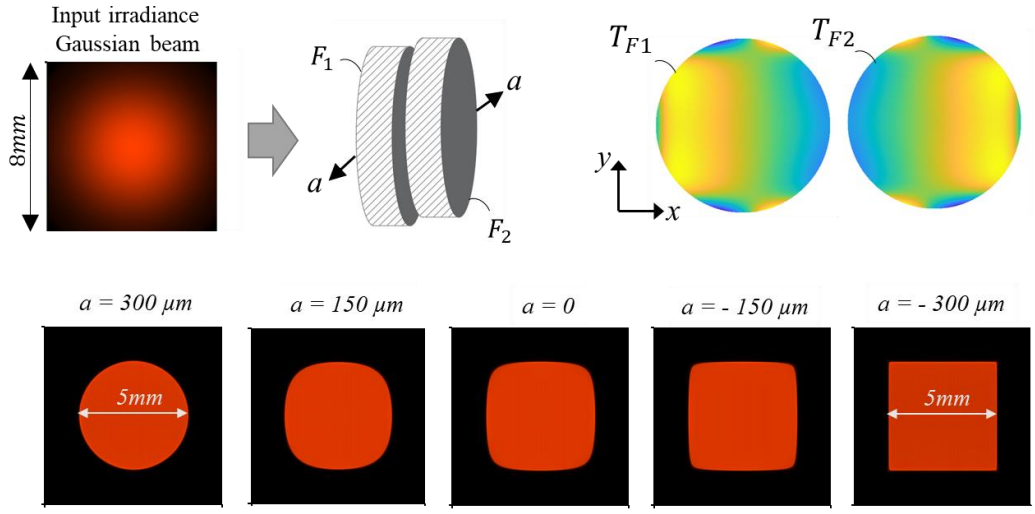

Fig. 4.11. Freeform surface geometries and simulated output irradiance patterns at 150 mm distance from dynamic-pattern beam shaper on an 8-by-8 mm detector.

4.5. Numerical design examples for dynamic freeform optics

As discussed in Section 4.3, the general dynamic design method we propose can also be implemented numerically for surfaces that are not conducive to analytical descriptions. The height maps of boundary elements are represented as thickness variations, $T_A(x, y)$ and $T_B(x, y)$ using point clouds for the calculation of the dynamic freeform pairs using Eqs. (4.8, 4.9) and numerical integration methods. We note that, in the default numerical implementation, the sizes of the dynamic plates will be the same as the boundary elements. Therefore, it may be useful to consider larger boundary lenses if they are equation based,

or to limit the aperture size in the dynamic system to ensure rays are passing through both freeform plates and have proper functionality. The maximum possible shift can be set initially based on the size of the boundary elements and then modified during the design process as the optical performance of the dynamic system is evaluated.

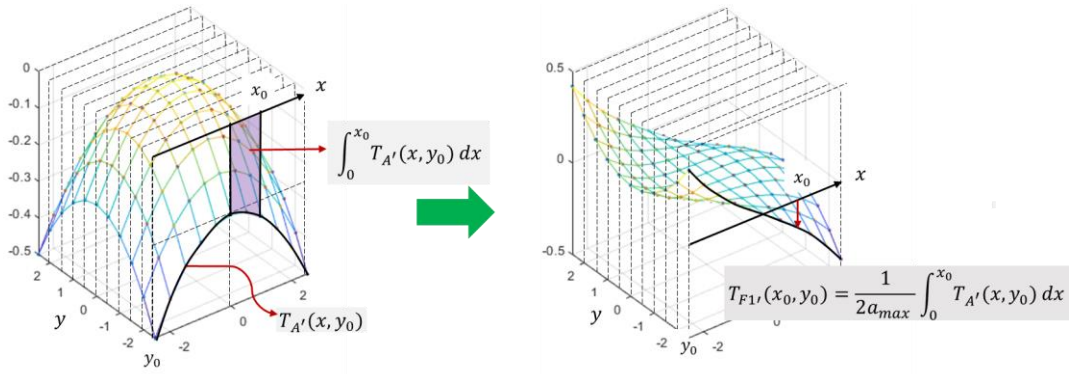

Fig. 4.12. Numerical integration approach applying the trapezoidal rule for proposed freeform design method.

The trapezoidal rule is a common method of performing numerical integration [40]. We developed a custom MATLAB™ code to accelerate the design process. To simplify the calculations, we reduced the integration dimension from 3D to 2D by discretizing the function along the *Y* axis and moving from *XYZ* space to *XZ* planes, as illustrated in Fig. 4.12. The cumulative integration for *x* with respect to zero was used at each *XZ* plane using the MATLAB™ "Cumtrapz" function. The accuracy of the numerical integration can be improved by increasing the number of surface points, but at the cost of increased computation time.

In this section we present three design examples solved using numerical methods. In the first example, we repeat the design of the variable positive-spherical power lens system from Section 4.4 using the numerical method and compare the outcomes. The second example considers a square to hexagonal dynamic pattern generator. The third example

demonstrates the flexibility of the general approach through a dynamic pattern generator that we believe would be impractical (or impossible) to implement with currently available analytical methods.

4.5.1 Numerical Example 1: Variable positive spherical power lens system

The boundary lenses for this design example are built from the first analytical example, as listed in Table 4.1. The point clouds of boundary lenses were generated in MATLAB™ with 0.05 mm resolution. By taking the thickness variation of the surface points and a maximum shift of 0.4 mm, dynamic freeform surface points were numerically generated in MATLAB™ using Eqs. (4.8, 4.9). We utilized the numerical integration approach discussed above. The MATLAB™ code was linked to LightTools™ to speed up analysis of the system's optical performance. Fig. 4.13 illustrates construction of the desired freeform plate geometry in LightToolsTM to match the geometry of the first analytical example.

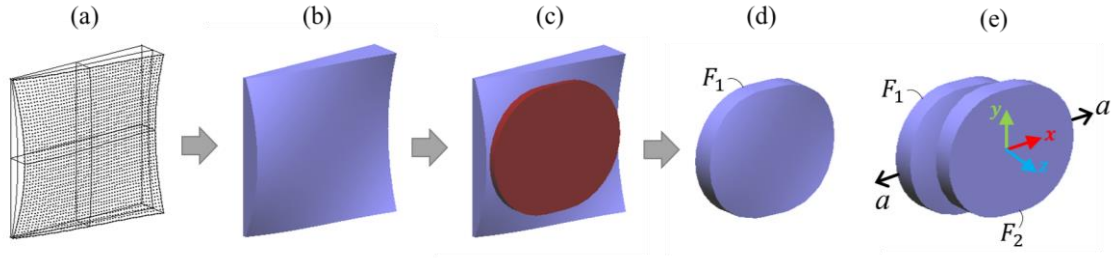

Fig. 4.13. (a) Constructing the freeform base plate in LightTools™ from MATLAB™ point cloud; (b) 3D model of freeform base, (c) intersecting freeform base with desired aperture geometry, (d) freeform plate with desired oval-shaped geometry, (e) 3D model of dynamic freeform system for first numerical example.

The optical power of the dynamic system was determined as the inverse of the back focal length at different lateral shifts using a parameter analyzer in LightTools™. The results obtained are in excellent agreement with the analytic results shown in Fig. 4.7. Table 4.4 compares the values obtained using the analytic and numerical approaches. The

differences increase slightly as the lateral shift is increased from zero to the maximum positive shift. In the case of maximum positive shift, the focal point expands to infinity, making the system extremely sensitive to lateral shift and resulting in a larger difference.

Table 4. 4 Optical power vs lateral shift for variable positive-power lens system

Lateral shift, *a (mm)* / Design method	0.399*	0.3	0.2	0.1	0	-0.1	-0.2	-0.3	-0.4
Power-Analytic (Diopters)	0.51	7.4	14.8	22.4	29.9	37.6	45.3	53.1	61.0
Power-Numerical (Diopters)	0.52	7.6	15.0	22.6	30.2	37.8	45.6	53.4	61.4
% Difference	1.9	2.7	1.3	0.9	0.7	0.7	0.6	0.6	0.7

*The focal point at 0.4 mm lateral shift goes to infinity, so we considered a slightly smaller shift value

4.5.2 Numerical Example 2: Simple dynamic pattern generator

Different numerical approaches to designing freeform lenses that allows for the generation of prescribed light distributions in illumination systems have recently been reviewed in the literature [24]. Recent advances in optical software also facilitate the numerically design of refractive elements to map the input light to a prescribed output light distribution. To this end, we used LightTools^{TM} Freeform Design (FFD) capability to create the boundary elements needed for this design example assuming the uniform plane wave source. In this example, we demonstrate the proposed numerical design method for a dynamic pattern generator changing the irradiance distribution between square and hexagonal target patterns.

The mesh grids of the resulting freeform surfaces were adjusted to uniform XY grids for compatibility with custom MATLAB^{TM} code developed to calculate the thickness variations of dynamic freeform plates. The boundary elements are 5 x 5 mm with 0.75 mm

thickness and a 4 x 4 mm uniform source. The design material and design wavelength are PMMA and 550 nm, respectively. The two boundary elements constructed in LightTools™ and the resulting illumination patterns 2 m from the first element interface are shown in Fig. 4.14.

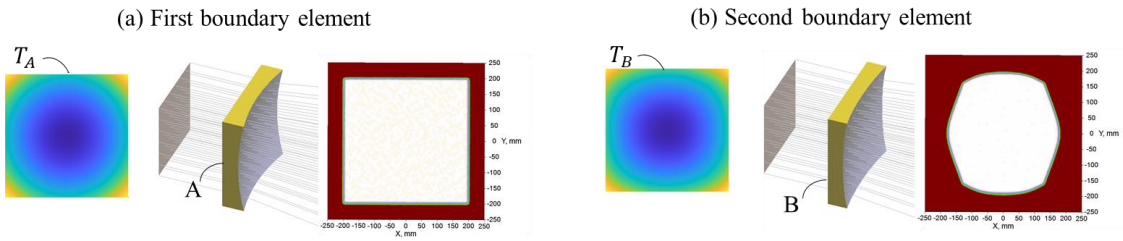

Fig. 4.14. Boundary elements of dynamic pattern generator producing (a) square, and (b) hexagonal patterns.

As in the previous example, the MATLAB™ code was linked to LightTools™ to import the surface height maps from the two boundary elements to accelerate the dynamic design process. Dynamic freeform point clouds were numerically calculated in MATLAB™ considering 200 by 200 mesh grids over the 5 mm x 5 mm mesh extent following Eqs. (4.8, 4.9) with a maximum shift of 0.2 mm. The resulting points were transferred to LightTools™ for optical performance evaluation as illustrated in Fig. 4.15 and Visualization 4.3. The aperture size and thicknesses of the freeform plates were assumed to be the same as the boundary elements. A 500 µm air gap was set between the freeform plates to avoid collision during shifting.

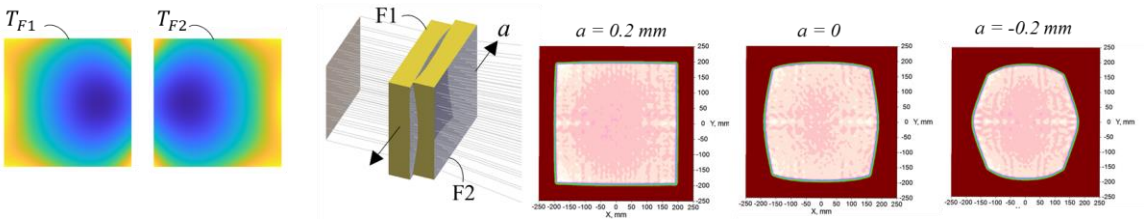

Fig. 4.15. Dynamic pattern generator varying from square to hexagonal pattern with applied lateral shift.

Numerical Example 3: Complex dynamic pattern generator

The results obtained from the previous example could arguably be achieved using analytic representations of the target patterns. For this reason, we repeated the process with the same design parameters but for significantly more complex target patterns that are not feasible to represent in analytic form. The two boundary elements constructed in LightTools™ and the resulting illumination patterns are shown in Fig. 4.16. The resulting dynamic system performance between the two boundaries is shown in Fig. 4.17 and Visualization 4.4. These results demonstrate the feasibility of the proposed general design method for dynamic freeform optical systems and show the potential for novel applications.

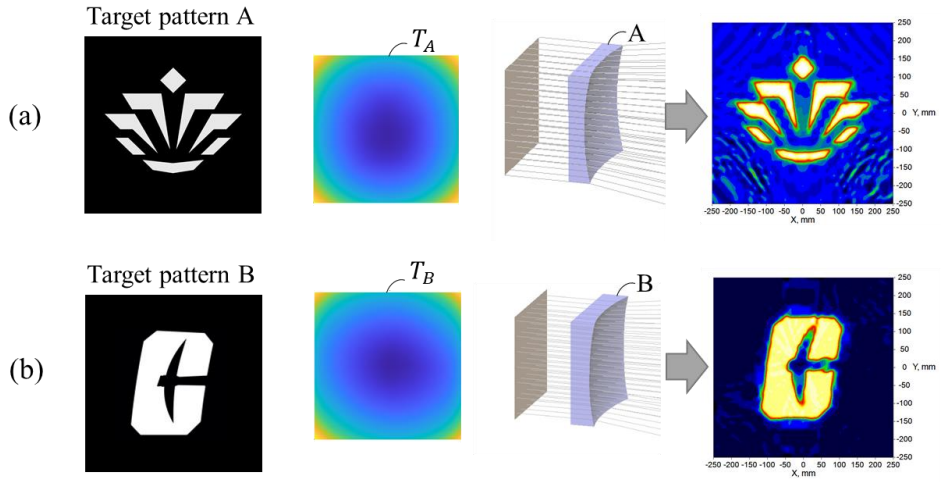

Fig. 4.16. (a) First and (b) second boundary elements and performance for complex illumination patterns.

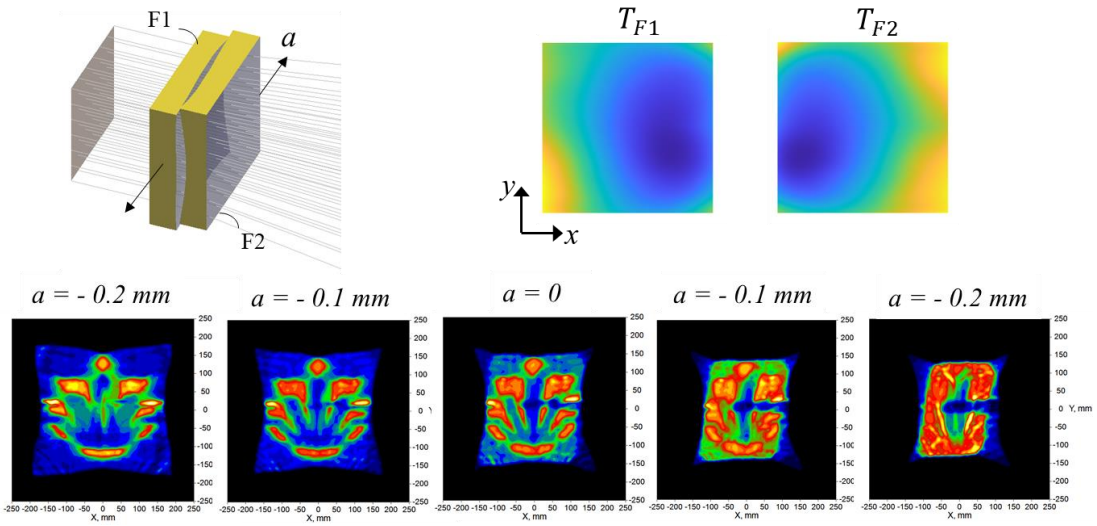

Fig. 4.17. Dynamic pattern generator varying between two complex illumination patterns with applied lateral shift.

4.6 Conclusions

We have presented accessible dynamic freeform design techniques for refractive two-element system that allows for varying optical performance between two defined boundary conditions. Similar to the Alvarez lens, pairs of plano-freeform elements are subjected to small, relative lateral shifts in opposing directions. The surface prescriptions of the boundary lenses, as well as the maximum desired shift between freeform plates, serve as the primary design inputs. This approach has advantages over prior methods in that it is not restricted to boundaries with similar optical functions and may be used to create a broad variety of challenging dynamic functions for both imaging and non-imaging applications. Depending on the characteristics of the boundary elements, this generalized technique can be implemented analytically or numerically. The analytical method is preferable if the boundary elements are easily specified using integrable surface equations without the need for surface fitting. Numerical approaches are useful when surface fitting would otherwise be required, and when boundary surface equations are available but problematic to integrated or to otherwise implement in optical software.

This general method was investigated and validated through multiple analytical and numerical design examples. The dynamic freeform systems utilized in the design examples were computed in MATLAB^{TM} using the general formula reported in this paper and their optical performance was determined using commercial optical design tools. The simulation results for all design examples are quite promising, even though no additional optical system adjustments or optimizations were performed. We note that that the dynamic beam shaper example designed using the analytical approach and the dynamic pattern generator designed using the numerical approach would be difficult or impossible to create with previously available design approaches, demonstrating the utility of the proposed method.

4.7 References

1. J. P. Rolland, M. A. Davies, T. J. Suleski, C. Evans, A. Bauer, J. C. Lambropoulos, and K. Falaggis, "Freeform optics for imaging," Optica 8, 161-176 (2021).
2. L. W. Alvarez and W. E. Humphrey, "Variable-power lens and system," U.S. patent 3,507,565A (21 April 1970).
3. J. G. Baker, "Variable power, analytic function, optical component in the form of a pair of laterally adjustable plates having shaped surfaces, and optical systems including such components," U.S. patent 3,583,790 (8 June 1971).
4. N. Matsuura, M. Kanno, H. Takeuchi and A. Ishikawa, "Endoscope with variable illumination angle," U.S. patent 4,736,734 (12 April 1988).
5. L. Kleinburg and M.J. Danley, "Variable shutter illumination system for microscope," U.S. patent 5,299,053 (29 March 1994).

6. S. S. Rege, T. S. Tkaczyk, and M. R. Descour, "Application of the Alvarez-Humphrey concept to the design of a miniaturized scanning microscope," Opt. Express 12(12), 2574-2588 (2004).
7. I. A. Palusinski, J. M. Sasián, and J. E. Greivenkamp, "Lateral-shift variable aberration generators," Appl. Opt. 38(1), 86-90 (1999).
8. S. Moein and T. J. Suleski, "Freeform optics for variable extended depth of field imaging," Opt. Express 29(24), 40524-40537 (2021).
9. J. Koerber, G.D. Boreman, and T.J. Suleski, "Broadband Variable Transmission Sphere for Fizeau Interferometry," Optics 3, 88-98 (2022).
10. A. Wilson and H. Hua, "Design and demonstration of a vari-focal optical see-through head-mounted display using freeform Alvarez lenses," Opt. Express 27(11), 15627-15637 (2019).
11. S. Shadalou, W. J. Cassarly, and T. J. Suleski, "Tunable illumination for LED-based systems using refractive freeform arrays," Opt. Express 29(22), 35755-35764 (2021).
12. A. G. Poullain and D. H. J. Cornet, "Optical lens," U.S. patent 1,143,316 (15 June 1915).
13. H. J. Birchall, "Lens of variable focal power having surfaces of involute form," U.S. patent 2,475,275 (5 July 1949).
14. E. C. Ernest, "Spectacle lens," U.S. patent 2,109,474 (1 March 1938).
15. D. Y. Zhang, V. Lien, Y. Berdichevsky, J. Choi, and Y. H. Lo, "Fluidic adaptive lens with high focal length tunability," Appl. Phys. Lett. 82(19), 3171-3172 (2003).
16. H. Ren and S. T. Wu, "Variable-focus liquid lens," Opt. Express 15(10), 5931-5936 (2007).

17. N. T. Nguyen, “Micro-optofluidic Lenses: A review,” Biomicrofluidics 4(3), 031501 (2010).
18. B. Berge and J. Peseux, “Variable focal lens controlled by an external voltage: An application of electrowetting,” Eur. Phys. J. E 3(2), 159-163 (2000).
19. S. Sato, “Liquid-crystal lens-cells with variable focal length,” Jpn. J. Appl. Phys. 18(9), 1679 (1979).
20. M. Ye and S. Sato, “Optical properties of liquid crystal lens of any size,” Jpn. J. Appl. Phys. 41(5B), L571 (2002).
21. H. C. Lin, M. S. Chen, and Y. H. Lin, “A review of electrically tunable focusing liquid crystal lenses,” Trans. Electr. Electron. Mater. 12(6), 234-240 (2011).
22. E. I. Betensky, J. B. Caldwell, I. A. Neil, and T. Yamanashi, “Zoom lens system,” U.S. patent 6,961,188 B2 (1 Nov. 2005).
23. T. Yamanashi, “Wide angle zoom lens,” U. S. 8,503,102 B2 (6 Aug. 2013).
24. W. Li, S. Wei, Z. Fan, Z. Zhu, and D. Ma, “Variable-diameter beam-shaping system design with high zoom ratio containing aspheric optical components,” App. Opt. 60(3), 705-713 (2021).
25. I. Kitajima, "Improvements in lenses," U. K. patent 250, 268 (29 July1926).
26. S. F. Hou, "Lighting system with an adjustable illuminated area," U.S. patent 7,845,834 B2 (7 December 2010).
27. H. J. Birchall, "Lenses and their combination and arrangement in various instruments and apparatus," U.S. patent 2,001,952 (21 May1935).
28. A. W. Lohmann, "A New Class of Varifocal Lenses," Appl. Opt. 9(7), 1669-1671 (1970).

29. E. Acosta and J. Sasian, "Micro-Alvarez lenses for a tunable-dynamic-range Shack–Hartmann wavefront sensor," Japanese Journal of Appl. Physics 53(8S2), 08MG04 (2014).
30. P. J. Smilie and T. J. Suleski, "Variable-diameter refractive beam shaping with freeform optical surfaces." Opt. Lett. 36, 4170-4172 (2011).
31. T. J. Suleski, J. A. Shultz, and P. J. Smilie, "Design of Dynamic Freeform Optics," in Renewable Energy and the Enviroment, (Optical publishing group, 2013), paper FW2B.2.
32. T. J. Suleski, Jason A. Shultz, and Paul J. Smilie, "Dynamic beam shaping with freeform optics," Proc. SPIE 9194, 91940K (2014).
33. T. J. Suleski, P.J. Smilie, and J. A. Shultz, "Dynamic laser beam shaping methods and systems," U.S. patent 9,238,577 B2 (19 January 2016).
34. R. Wu, Z. Feng, Z. Zheng, R. Liang, P. Benítez, J. C. Miñano, and F. Duerr, "Design of Freeform Illumination Optics," Laser Photonics Rev. 12(7), 1700310 (2018).
35. Y. Ding, X. Liu, Z. Zheng, and P. Gu, "Freeform LED lens for uniform illumination," Opt. Express 16(17)12958-12966 (2008).
36. F. R. Fournier, W. J. Cassarly, and J. P. Rolland, "Designing freeform reflectors for extended sources," Proc. SPIE 7423, 742302 (2009).
37. Z. Zhenrong, H. Xiang, and L. Xu, "Freeform surface lens for LED uniform illumination," Appl. Optics, 48(35), 6627-6634 (2009).
38. J. J. Chen, T. Y. Wang, K. L. Huang, T. S. Liu, M. D. Tsai, and C. T. Lin, "Freeform lens design for LED collimating illumination," Opt. Express 20(10), 10984-10995 (2012).

39. R. Hu, Z. Gan, X. Luo, H. Zheng, and S. Liu, "Design of double freeform-surface lens for LED uniform illumination with minimum Fresnel losses," Optik 124(19), 3895-3897 (2013).

40. R. Wu, P. Liu, Y. Zhang, Z. Zheng, H. Li, and X. Liu, "A mathematical model of the single freeform surface design for collimated beam shaping," Opt. Express 21(18), 20974-20989 (2013).

41. X. Mao, H. Li, Y. Han, and Y. Luo, "Two-step design method for highly compact three-dimensional freeform optical system for LED surface light source," Opt. Express 22(S6), A1491-A1506 (2014).

42. D. Ma, Z. Feng, and R. Liang, "Tailoring freeform illumination optics in a double-pole coordinate system," Appl. Optics 54(9), 2395-2399 (2015).

43. X. Hui, J. Liu, Y. Wan, and H. Lin, "Realization of uniform and collimated light distribution in a single freeform-Fresnel double surface LED lens," Appl. Optics 56(15), 4561-4565 (2017).

44. P. Benítez , R. M. Arroyo, and J. C. Miñano , "Design in 3D geometry with the simultaneous multiple surface design method of nonimaging optics," Proc. SPIE 3781, 12-21 (1999).

45. J. C. Miñano, P. Benítez, J. Blen, "High-efficiency free-form condenser overcoming rotational symmetry limitations," Opt. Express 16(25), 20193-20205 (2008).

46. F. Chen, S. Liu, K. Wang, Z. Liu, and X. Luo, "Free-form lenses for high illumination quality light-emitting diode MR16 lamps," Opt. Eng. 48, 123002 (2009).

47. J. Y. Cai, Y. C. Lo, and C. C. Sun, "Optical design of the focal adjustable flashlight based on a power white-LED," Proc. SPIE 8128, 812806 (2011).

48. E. Juntunen, P. Myöhänen, E. Tetri, O. Tapaninen, J. Ojalehto, and V. Heikkinen, "Rapid prototyping of freeform optics for an LED downlighter with a dynamically adjustable beam," Light. Res. Technol. 48(7), 885-897 (2016).
49. J. A. Shultz, "Design, tolerancing, and experimental characterization of dynamic freeform optical systems," Ph.D. dissertation (The University of North Carolina at Charlotte, 2017).
50. T. A. Driscoll and R. J. Braun, Fundamental of Numerical computation (SIAM, 2017), Chap. 5.

CHAPTER 5: CONCLUSION

5.1 Summary of work

The design and characterization of novel freeform designs to enable spatial light distribution with continuously variable sizes or shapes in illumination systems have been presented in this dissertation.

In Chapter 2, a novel system based on arrays of freeform varifocal Alvarez lenses was reported that enables continuous change of illumination size with high uniformity with an LED source. Convergent ray bundles were used to illuminate the Alvarez arrays to extend the working range of the Alvarez elements. The design demonstrated dynamic illumination from spot mode to uniform square-shape flood mode through millimeter-scale lateral shifts between the Alvarez arrays. The system design was initialized using paraxial geometrical optics concepts and then refined for a white LED source through a multi-step optimization process. The square lens arrays in this system enabled the square light output for the flood mode. Simulations showed that the system met the desired performance goals with good uniformity. The demonstrated design approach is beneficial for applications where system size and dynamic range of physical movement are restricted, and non-circular output patterns are desired.

Chapter 3 reported on the experimental realization and characterization of a variable illumination system designed using methods presented in Chapter 2. A commercially available TIR lens was employed in the design to create convergent ray bundle inputs to the custom Alvarez arrays and to decrease the cost and shorten the system build time. A novel camera-based test station was developed and calibrated along with custom analysis software to assess the optical performance of the demonstrator. Some small differences

between simulated and experimental results were noticed, which we believe were due to uncertainties in estimated geometrical parameters of the COTS TIR lens model. However, the experimental results demonstrated and confirmed the dynamic illumination concept with good uniformity.

Chapter 4 focused on simplifying and generalizing the design of dynamic freeform optics to enable variable functionality for illumination and imaging systems. A general design method for a refractive two-element system was presented that enables variable optical performance between two specified boundaries. As with Alvarez lenses, the plano-freeform pairs were subjected to relatively small lateral shifts in opposing directions. Multiple analytical and numerical design examples were used to explore and validate this general method. The dynamic freeform system examples were calculated in MATLAB™ and the optical performance evaluated using commercial optical design tools. Even though no additional optimizations were made, the simulation results were highly encouraging for all of the design examples. In particular, the dynamic pattern beam shaper example created with the analytical approach and the dynamic pattern generator example created numerically would be difficult or impossible to build using previously available design methodologies. This new design method has demonstrated great potential for novel optical applications for both illumination and imaging.

5.2 Future work

1. Rotational configurations can simplify the packaging and alignment challenges for tunable freeform elements. Additional study of system geometries and design methods for rotational freeform may be beneficial.

2. Investigate additional types of mechanical and electrical actuators to achieve the opposite shifts between freeform pairs for dynamic illumination.

3. The general dynamic freeform design method was demonstrated for varying optical functionality between two boundaries with relative shifts applies to freeform components along the X axis. The method and capabilities might be further generalized by exploring relative shifts along both X and Y axes.

4. In this work, the dynamic freeform designs in the numerical implementation of the general dynamic freeform design method are calculated using the XYZ coordinates of point clouds from the boundary surfaces and trapezoidal integration. Adding the normal orientation of the surface at each point and use of more advanced numerical integration methods may enable more precise surface prescriptions.

REFERENCES

1. R. Winston, J. C. Miñano, P. G. Benitez, *Nonimaging Optics* (Elsevier Science & Technology, 2005).

2. R. J. Koshel, *Illumination Engineering: design with nonimaging optics* (John Wiley & Sons, 2012), Chap. 1.

3. A. V. Arecchi, R. J. Koshel, and T. Messadi, *Field guide to illumination* (SPIE, 2007).

4. W. J. Cassarly and M.J. Hayford, "Illumination optimization: The revolution has begun," International Optical Design Conference, Vol. 4832, SPIE (2002).

5. A. J. Whang, S. Chao, C. Chen, Y. Chen, H. Hsiao, and X. Hu, "High uniform illumination of light-emitting diodes lighting with applying the multiple-curvature lens," Opt. Rev. 18(2), 218-223 (2011).

6. W. S. Lee, "Zoomable LED flashlight," U. S. patent 9,068,727 B2 (30 June 2015).

7. R. D. White and D.P. Weiss, "Lighting device with dynamic bulb position," U. S. patent 4,339,788 (13 Jul. 1982).

8. J. Koehler, and J. Wangler, "Zoom system for an illumination device," U.S. patent 6,864,960 B2 (8 March 2005).

9. D. Y. Zhang, V. Lien, Y. Berdichevsky, J. Choi, and Y. H. Lo, "Fluidic adaptive lens with high focal length tunability," Appl. Phys. Lett. 82(19), 3171-3172 (2003).

10. A. Werber and H. Zappe, "Tunable microfluidic microlenses," Appl. Opt. 44(16), 3238-3245 (2005).

11. H. Ren and S. T. Wu, "Variable-focus liquid lens," Opt. Express 15(10), 5931-5936 (2007).

12. N. T. Nguyen, "Micro-optofluidic Lenses: A review," Biomicrofluidics 4(3), 031501 (2010).

13. B. Berge and J. Peseux, "Variable focal lens controlled by an external voltage: An application of electrowetting," Eur. Phys. J. E 3(2), 159-163 (2000).

14. S. Sato, "Liquid-crystal lens-cells with variable focal length," Jpn. J. Appl. Phys. 18(9), 1679 (1979).

15. D. W. Berreman, "Variable focus liquid crystal lens system," U.S. patent 4,190,330 (26 Feb. 1980).

16. S. Sato, “Applications of liquid crystals to variable-focusing lenses,” Opt. Rev. 6(6), 471-485 (1999).

17. M. Ye and S. Sato, “Optical properties of liquid crystal lens of any size,” Jpn. J. Appl. Phys. 41(5B), L571 (2002).

18. H. C. Lin, M. S. Chen, and Y. H. Lin, “A review of electrically tunable focusing liquid crystal lenses,” Trans. Electr. Electron. Mater. 12(6), 234-240 (2011).

19. Z. Yongchao, “Development of solid tunable optics for ultra-miniature imaging systems,” Ph.D. dissertation (National University of Singapore, 2016).

20. G. Beadie, M. L. Sandrock, M. J. Wiggins, R. S. Shirk, M. Ponting, Y. Yang, T. Kazmierczak, A. Hiltner, and E. Baer, “Tunable polymer lens,” Opt. Express 16(16), 11847-11857 (2008).

21. S. Y. Lee, H. W. Tung, W. C. Chen, and W. Fang, “Thermal actuated solid tunable lens,” IEEE Photonics Technol. Lett. 18(21), 2191-2193 (2006).

22. P. Liebetraut, S. Petsch, W. Mönch, and H. Zappe, “Tunable solid-body elastomer lenses with electromagnetic actuation,” Appl. Optics 50(19), 3268-3274 (2011).

23. J. B. Lee, B. I. Chiang, H. K. Ho, “Zoom spotlight using LED array,” U.S. patent 8,979,316 B2 (17 March 2015).

24. M. Sommers and J.T. Petroski, “Zoomable spot module,” U.S. patent 6,866,401 B2 (15 March 2005).

25. A. J. Whang, Y. Y. Chen, and Y. T. Teng, “Designing uniform illumination systems by surface-tailored lens and configurations of LED arrays,” J. Disp. Technol. 5(3), 94-103 (2009).

26. M. Bueeler and M. Aschwanden, “Illumination source with variable divergence,” U.S. patent 8,944,647 B2 (3 Feb 2015).

27. I. Harder, M. Lano, N. Lindlein, J. Schwider, “Homogenization and beam shaping with microlens arrays,” Photonics Europe, Vol. 5456, 99-107, SPIE (2007).

28. O. Homburg, L. Aschke, and V. Lissotschenko, “Refractive microlens structures with high-damage thresholds enable flexible beam shaping of high-power lasers,” Laser-Induced Damage in Optical Materials, Vol. 6403, 660-666, SPIE (2007).

29. T. R. Sales, “Random microlens array for optical beam shaping and homogenization,” U.S. patent 6,859,326 B2 (22 Feb 2005).

30. F. C. Wippermann, P. Dannberg, A. Bräuer, S. Sinzinger, “Improved homogenization of fly's eye condenser setups under coherent illumination using chirped microlens arrays,” MOEMS and Miniaturized Systems VI, Vol. 6466, 241-249, SPIE (2007).

31. M. Zimmermann, N. Lindlein, R. Voelkel, K. J. Weible, “Microlens laser beam homogenizer: from theory to application,” Laser Beam Shaping VIII, Vol. 6663, SPIE (2007).

32. H. Ries and A. Rabl, “Edge-ray principle of nonimaging optics,” J. Opt. Soc. Am. A 11(10), 2627-2632 (1994).

33. Riser, A.P. and W.J. Cassarly, “Analysis of single lens arrays using convolution,” Opt. Eng. 40(5), 805-813 (2001).

34. E. Savio, L. D. Chiffre, and R. Schmitt, “Metrology of freeform shaped parts,” CIRP annals 56(2), 810-835 (2007).

35. F. Z. Fang, X. D. Zhang, A. Weckenmann, G. X. Zhang, C. Evans, “Manufacturing and measurement of freeform optics,” CIRP Annals 62(2), 823-846 (2013).

36. L. Zhang, G. Liu, X. Zhao, O. Dambon, F. Klocke, “Precision molding of optics: a review of its development and applications,” Polymer Optics and Molded Glass Optics: Design, Fabrication, and Materials 9949, 34-40 (2016).

37. L. Zhang, Z. Li, F. Fang, S. Huang, X. Zhang, “Review on fast tool servo machining of optical freeform surfaces,” Int. J. Adv. Manuf. Technol. 95(5), 2071-2092 (2018).

38. J. P. Rolland, M. A. Davies, T. J. Suleski, C. Evans, A. Bauer, J. C. Lambropoulos, and K. Falaggis, "Freeform optics for imaging," Optica 8, 161-176 (2021).

39. I. Kitajima, "Improvements in lenses," U. K. patent 250, 268 (29 July1926).

40. H. J. Birchall, "Lenses and their combination and arrangement in various instruments and apparatus," U.S. patent 2,001,952 (21 May 1935).

41. R. W. Lewis, “Lens and method of producing it,” U.S. patent 2,263,509 (18 Nov. 1941).

42. S. F. Hou, "Lighting system with an adjustable illuminated area," U.S. patent 7,845,834 B2 (7 December 2010).

43. L. W. Alvarez and W. E. Humphrey, "Variable-power lens and system," U.S. patent 3,507,565A (21 April 1970).

44. A. W. Lohmann, "A New Class of Varifocal Lenses," Appl. Opt. 9(7), 1669-1671 (1970).

45. J. G. Baker, "Variable power, analytic function, optical component in the form of a pair of laterally adjustable plates having shaped surfaces, and optical systems including such components," U.S. patent 3,583,790 (8 June 1971).

46. J. G. Baker, and W.T. Plummer, “Analytic function optical component,” U.S. patent 4,650,292 (17 March 1987).

47. Barbero, S., “The Alvarez and Lohmann refractive lenses revisited,” Opt. Express 17(11), 9376-9390 (2009).

48. P. J. Smilie, T. J. Suleski, B. Dutterer, J. L. Lineberger, M. A. Davies, “Design and characterization of an infrared Alvarez lens,” Opt. Eng. 51(1), SPIE (2012).

49. D. Crosby, G. Storey, R. Taylor, O. Reading, “Adjustable refractive optical device,” U.S. patent 9,335,446 B2 (10 May 2016).

50. I. A. Palusinski, J. M. Sasián, and J. E. Greivenkamp, "Lateral-shift variable aberration generators," Appl. Opt. 38(1), 86-90 (1999).

51. J. A. Shultz, "Design, tolerancing, and experimental characterization of dynamic freeform optical systems," Ph.D. dissertation (The University of North Carolina at Charlotte, 2017).

52. S. Petsch, A. Grewe, L. Köbele, S. Sinzinger, and H. Zappe, “Ultrathin Alvarez lens system actuated by artificial muscles,” Appl. Optics 55(10), 2718-2723, (2016).

53. A. Grewe, M. Hillenbrand, and S. Sinzinger, “Aberration analysis of optimized Alvarez-Lohmann lenses,” Appl. Optics 53(31), 7498-7506 (2014).

54. G. Zhou, H. Yu, and F.S. Chau, “Microelectromechanically-driven miniature adaptive Alvarez lens,” Opt. Express 21(1), 1226-1233 (2013).

55. E. Acosta and J. Sasian, “Micro-Alvarez lenses for a variable dynamic range Shack-Hartmann wavefront sensor,” Eighteenth Microoptics Conference (2013).

56. E. Acosta and J. Sasian, "Micro-Alvarez lenses for a tunable-dynamic-range Shack–Hartmann wavefront sensor," Jpn. J. Appl. Phys. 53(8S2), 08MG04 (2014).

57. L. Sun, S. Jin, and S. Cen, “Free-form microlens for illumination applications,” Appl. Optics 48(29), 5520-5527 (2009).

58. R. Wu, Z. Feng, Z. Zheng, R. Liang, P. Benítez, J. C. Miñano, and F. Duerr, "Design of Freeform Illumination Optics," Laser Photonics Rev. 12(7), 1700310 (2018).

59. Y. Ding, X. Liu, Z. Zheng, and P. Gu, "Freeform LED lens for uniform illumination," Opt. Express 16(17), 12958-12966 (2008).

60. Z. Zhenrong, H. Xiang, and L. Xu, "Freeform surface lens for LED uniform illumination," Appl. Optics, 48(35), 6627-6634 (2009).

61. L. Wang, K. Qian, and Y. Luo, "Discontinuous free-form lens design for prescribed irradiance," Appl. Opt. 46(18), 3716-3723 (2007).

62. A. Bruneton, A. Bäuerle, R. Wester, J. Stollenwerk, P. Loosen, "Limitations of the ray mapping approach in freeform optics design," Opt. Lett. 38(11), 1945-1947 (2013).

63. D. Ma, Z. Feng, and R. Liang, "Tailoring freeform illumination optics in a double-pole coordinate system," Appl. Optics 54(9), 2395-2399 (2015).

64. J. S. Schruben, "Formulation of a Reflector-Design Problem for a Lighting Fixture," J. Opt. Soc. Am. 62(12), 1498-1501 (1972).

65. R. Wu, P. Benítez, Y. Zhang, C. Miñano, Influence of the characteristics of a light source and target on the Monge-Ampère equation method in freeform optics design. Opt. Lett. 39(3), 634-637 (2014).

66. S. Chang, R. Wu, L. An, Z. Zheng, "Design beam shapers with double freeform surfaces to form a desired wavefront with prescribed illumination pattern by solving a Monge-Ampère type equation," J. Opt. 18(12), 125602 (2016).

67. V. Oliker, "Freeform optical systems with prescribed irradiance properties in near-field," International Optical Design Conference, Vol. 6342, SPIE (2006).

68. K. V. Andreeva, S. V. Kravchenko, m. A. Moiseev, and L. L. Doskolovich, "Designing freeform TIR optical elements using supporting quadric method," Opt. Express 25(19), 23465-23476 (2017).

69. T. L. R. Davenport, T.A. Hough, and W.J. Cassarly, "Optimization for illumination systems: the next level of desig," Photon Management, Vol.5456, 81-90 (2004).

70. Z. Liu, P. Liu, and F. Yu, "Parametric optimization method for the design of high-efficiency free-form illuminationsystem with a LED source", Chin. Opt. Lett. 10(11), 112201-112201 (2012).

71. X. Mao, H. Li, Y. Han, and Y. Luo, "Two-step design method for highly compact three-dimensional freeform optical system for LED surface light source," Opt. Express 22(S6), A1491-A1506 (2014).

72. P. Benítez , R. M. Arroyo, and J. C. Miñano , "Design in 3D geometry with the simultaneous multiple surface design method of nonimaging optics," Proc. SPIE 3781, 12-21 (1999).

73. J. C. Miñano, P. Benítez, J. Blen, "High-efficiency free-form condenser overcoming rotational symmetry limitations," Opt. Express 16(25), 20193-20205 (2008).

74. J. Y. Cai, Y. C. Lo, and C. C. Sun, "Optical design of the focal adjustable flashlight based on a power white-LED," Proc. SPIE 8128, 812806 (2011).

75. E. Juntunen, P. Myöhänen, E. Tetri, O. Tapaninen, J. Ojalehto, and V. Heikkinen, "Rapid prototyping of freeform optics for an LED downlighter with a dynamically adjustable beam," Light. Res. Technol. 48(7), 885-897 (2016).

76. Xin, D., et al., Design of secondary optics for IRED in active night vision systems. Opt. Express 21(1), 1113-1120 (2013).

77. P. J. Smilie and T. J. Suleski, "Variable-diameter refractive beam shaping with freeform optical surfaces." Opt. Lett. 36, 4170-4172 (2011).

78. T. J. Suleski, J. A. Shultz, and P. J. Smilie, "Design of Dynamic Freeform Optics," in Renewable Energy and the Enviroment, (Optica publishing group, 2013), paper FW2B.2.

79. T. J. Suleski, Jason A. Shultz, and Paul J. Smilie, "Dynamic beam shaping with freeform optics," Proc. SPIE 9194, 91940K (2014).

80. T. J. Suleski, P.J. Smilie, and J. A. Shultz, "Dynamic laser beam shaping methods and systems," U.S. patent 9,238,577 B2 (19 January 2016).

81. S. Shadalou, W. J. Cassarly, and T. J. Suleski, "Tunable illumination for LED-based systems using refractive freeform arrays," Opt. Express 29(22), 35755-35764 (2021).

82. S. Shadalou and T. J. Suleski, "General design method for dynamic freeform optics with variable functionality," Opt. Express 30, 19974-19989 (2022).